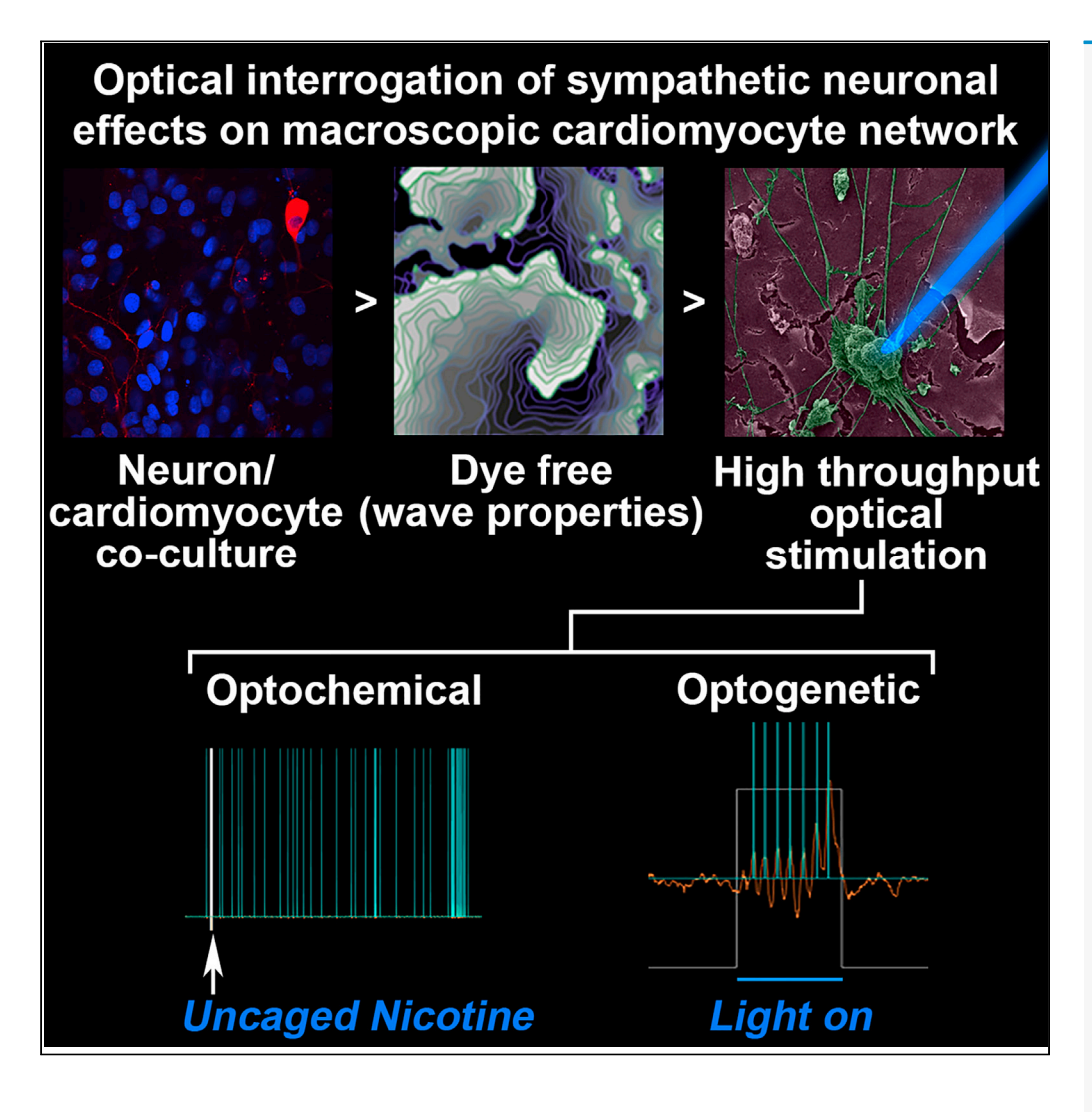
iScience



Article

Optical Interrogation of Sympathetic Neuronal Effects on Macroscopic Cardiomyocyte Network Dynamics



Rebecca-Ann B. Burton, Jakub Tomek, Christina M. Ambrosi, ..., Emilia Entcheva, David J. Paterson, Gil Bub

rebecca.burton@pharm.ox.ac uk (R.-A.B.B.) gil.bub@mcgill.ca (G.B.)

HIGHLIGHTS

A methodology to study neuron-cardiac interactions at multicellular/tissue level

Cardiac sympathetic stellate neurons can alter cardiac wave stability

Optogenetic control of sympathetic neurons offers temporal and spatial control

Increasing neuron density in co-cultures affects cardiac firing frequency

Burton et al., iScience 23, 101334 July 24, 2020 © 2020 The Authors. https://doi.org/10.1016/ j.isci.2020.101334



iScience



Article

Optical Interrogation of Sympathetic Neuronal Effects on Macroscopic Cardiomyocyte Network Dynamics

Rebecca-Ann B. Burton, ^{1,2,8,9,*} Jakub Tomek, ^{2,8} Christina M. Ambrosi, ³ Hege E. Larsen, ² Amy R. Sharkey, ² Rebecca A. Capel, ¹ Alexander D. Corbett, ⁴ Samuel Bilton, ² Aleksandra Klimas, ³ Guy Stephens, ² Maegan Cremer, ¹ Samuel J. Bose, ¹ Dan Li, ² Giuseppe Gallone, ^{2,5} Neil Herring, ² Edward O. Mann, ² Abhinav Kumar, ⁶ Holger Kramer, ² Emilia Entcheva, ³ David J. Paterson, ² and Gil Bub^{2,7,*}

SUMMARY

Cardiac stimulation via sympathetic neurons can potentially trigger arrhythmias. We present approaches to study neuron-cardiomyocyte interactions involving optogenetic selective probing and all-optical electrophysiology to measure activity in an automated fashion. Here we demonstrate the utility of optical interrogation of sympathetic neurons and their effects on macroscopic cardiomyocyte network dynamics to address research targets such as the effects of adrenergic stimulation via the release of neurotransmitters, the effect of neuronal numbers on cardiac behavior, and the applicability of optogenetics in mechanistic *in vitro* studies. As arrhythmias are emergent behaviors that involve the coordinated activity of millions of cells, we image at macroscopic scales to capture complex dynamics. We show that neurons can both decrease and increase wave stability and re-entrant activity in culture depending on their induced activity—a finding that may help us understand the often conflicting results seen in experimental and clinical studies.

INTRODUCTION

Cardiac impulse formation and conduction are modulated by autonomic activity, and the autonomic nervous system plays an important role in the initiation and maintenance of arrhythmias in diseased hearts (Bub and Burton, 2014; Herring et al., 2019; Winfree, 1987). Sympathetic nerves release noradrenaline, which activates cardiac β -adrenergic receptors to modulate myocyte repolarization and calcium handling via alterations of transmembrane currents and intracellular calcium homeostasis (Bers, 2008; Zaccolo and Pozzan, 2002). Increased sympathetic activity, which can occur during epileptic seizures (Devinsky, 2004) and is also associated with chronic diseases such as hypertension (Julius, 1998) and heart failure (Cohn et al., 1984), is often associated with increased risk of re-entrant arrhythmias (Chen et al., 2014). Tissue damage can also alter the distribution of innervation where cardiac cell death following myocardial infarction causes sympathetic denervation followed by nerve sprouting and reinnervation (Gardner et al., 2016).

Nerve sprouting may promote the heterogeneity of excitability and refractoriness, which was suggested as a mechanism for increased arrhythmia susceptibility in the reinnervated infarct border zone (Cao et al., 2000; Chen et al., 2001). However, recent clinical studies (Boogers et al., 2010; Fallavollita et al., 2014, 2017; Nishisato et al., 2010; Standen et al., 1989; Vaseghi et al., 2012) have shown that cardiac sympathetic denervation (rather than reinnervation) can lead to a higher risk of ventricular arrhythmias and arrhythmic death. Experimental and computational studies linked the beneficial effect of innervation to attenuation of infarct-induced vulnerability to repolarization alternans via β -adrenergic activation (Tomek et al., 2017, 2019) or to reduction of electrophysiological heterogeneity and calcium mishandling, which was present even when the nerves were not activated (Gardner et al., 2015). Resolving the unclear pro- or antiarrhythmic effect of post-infarction reinnervation may also involve the precise understanding of neural heterogeneity and its role in arrhythmia modulation. Research on these questions may therefore benefit from the use of a cell culture model system where the effects of innervation can be precisely controlled. Co-cultures of cardiac myocytes and sympathetic neurons have been investigated for over 30 years (Furshpan et al., 1976;

¹University of Oxford, Department of Pharmacology, Mansfield Road, Oxford OX1 3QT, UK

²University of Oxford, Department of Physiology, Anatomy and Genetics, British Heart Foundation Centre of Research Excellence, Parks Road, Oxford OX1 3PT, UK

³The George Washington University, Department of Biomedical Engineering, Washington, DC 20052, USA

 $^4\mbox{University}$ of Exeter, Physics and Astronomy, Exeter EX4 4QL, UK

⁵Department of Computational Molecular Biology, Max Planck Institute for Molecular Genetics, Ihnestraße 63-73, 14195 Berlin, Germany

⁶University of Oxford, Department of Biochemistry, Glycobiology Institute, Oxford, UK

⁷McGill University, Department of Physiology, McIntyre Medical Sciences Building, Room 1128, 3655 Promenade Sir William Osler, Montréal, QC H3G 1Y6, Canada

⁸These authors contributed equally

⁹Lead Contact

*Correspondence: rebecca.burton@pharm.ox. ac.uk (R.-A.B.B.), gil.bub@mcgill.ca (G.B.) https://doi.org/10.1016/j.isci. 2020.101334







Horackova et al., 1993); however, these studies were carried out at microscopic (single cell) scales where arrhythmogenicity cannot be directly assessed. Tissue heterogeneity and impulse conduction velocity (CV) play key roles in the initiation and stability of re-entrant spiral waves (Winfree, 1987). Although CV depends in part on the excitability of individual myocytes, it also depends on cell-cell connectivity and tissue heterogeneity (Kleber and Rudy, 2004; Shaw and Rudy, 1997).

Confluent myocyte monocultures imaged at macroscopic space scales have allowed the investigation of more complex functional tissue level properties such as wave propagation and pattern formation (Entcheva and Bien, 2006; Tung and Zhang, 2006), and their ability to support reentrant spiral waves has validated their use as a model of arrhythmogenesis. Optical mapping of these cultures has given an insight into important arrhythmogenic mechanisms, including unidirectional conduction block, junctional coupling, and remodeling (Tung and Zhang, 2006). Confluent co-cultures of myocytes and neurons imaged at macroscopic scales (>1 cm²) are a potentially useful biological model system for the study of the proarrhythmic effects of abnormal sympathetic activation on cardiac conduction.

Recent studies have used optogenetic approaches to spatially control sympathetic activation to gain insights on communication dynamics between cardiomyocytes and neurons (Prando et al., 2018). In addition, a number of studies have quantified sympathetic axon density in healthy and diseased myocardium (Clarke et al., 2010; leda et al., 2007; Muhlfeld et al., 2010; Zhou et al., 2004), highlighting the relevance of neuron numbers and sympathetic miswiring in the diseased heart (Freeman et al., 2014). In this work, we report the first macroscopic optical mapping measurements of cardiac monolayers co-cultured with cardiac sympathetic stellate neurons imaged using our recently published dye-free optical imaging method (Burton et al., 2015). Further, in addition to the dye-free imaging experiments, we use another approach involving optogenetics combined with an automated system for high-throughput all-optical imaging as demonstrated in (Klimas et al., 2016, 2020) (OptoDyCE) to relate physical neuron-myocyte contacts to functional coupling between these cell populations and also quantify how neural stimulation modulates cardiac behavior, which may ultimately give insights pertinent to pathophysiological questions. Finally, we explored the effects of neuron numbers on cardiac behavior and their ability to modulate cardiac excitability.

RESULTS

1] Stellate Sympathetic Neurons Make Contacts with Cardiomyocytes

Scanning electron microscopy (SEM) of sympathetic neurons growing in co-culture with cardiomyocytes *in vitro* shows connections between neurite extension and cardiac syncytium (Figure 1A). The neuron bodies and extensions clearly make physical contact with myocytes. Close up of a connection between neurite extension and cardiac syncytium shows connections between neurons and myocytes (Figure 1B). Figures 1C–1F demonstrate that neuron bodies and extensions make contact with myocytes (white asterisk showing dendritic process, Figure 1E; white arrow indicating neuron body, Figure 1F). See also Figure S1 for wide-field SEM images showing extensive dendritic processes and arborization. Immunofluorescence staining of co-cultures demonstrated that sympathetic neurons showed positive staining for tyrosine hydroxylase (TH) (Figures S2 and S4), and fibroblast contamination in the co-cultures was assessed by staining with vimentin (Figure S3), which showed low abundance.

2] Neurite Extensions in Co-cultures of Sympathetic Neurons and Cardiomyocytes

Release from varicosities along the length of the dendrites would enable synchronized signaling to the myocytes. Neurite lengths were segmented, tabulated, and measured (Figures 2A(i) and S1). The average neurite length is computed as a weighted average: $1183.07 \pm 375.42 \, \mu m$. To estimate the average number of cardiac cell boundaries a dendritic process might encounter, we performed image analysis in a confocal image stack of fluorescently labeled cardiomyocytes (TH488) (Figure 2A(ii)). A maximum intensity projection was taken of the image stack before manually segmenting the cardiomyocyte (CM) cell boundaries (Figure 2A(iii)). One hundred random transects were calculated for the segmented image shown in Figures 2A(iii) and 2A(iv). The average number of cell boundaries encountered along these 50 μ m trajectories were N = 4.21 \pm 2.05. This provides an estimate of the distance between cell boundaries as being 50 μ m/N = 11.87 \pm 5.77 μ m. The simulation shows that a cell boundary is crossed every 12 \pm 6 μ m. For \sim 1,000 μ m of total neuron process length this corresponds to 1,000/(12 \pm 6) = 56–167 cell boundaries crossed i.e. \sim a maximum of 56–167 myocytes innervated.



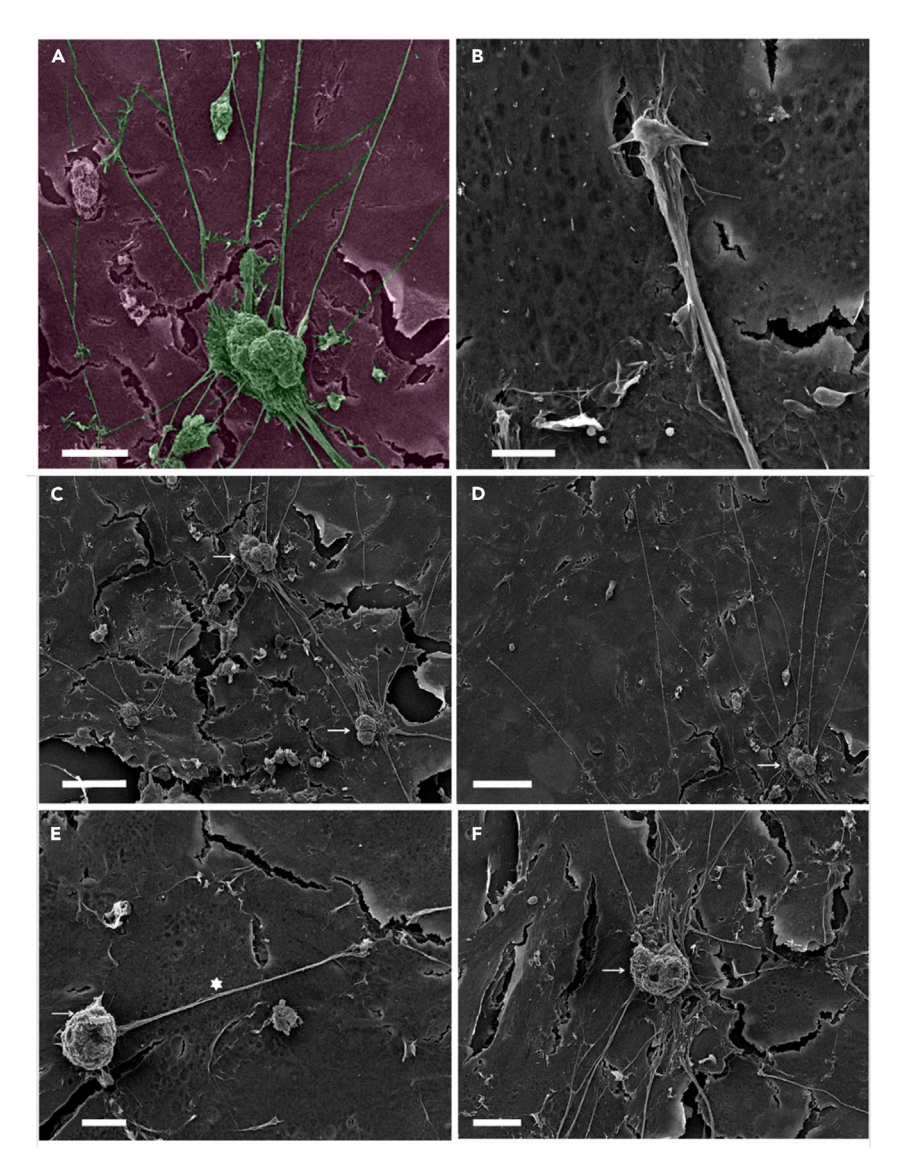


Figure 1. Scanning Electron Microscopy of Cardiac-Neuron Co-cultures

(A) Exemplar image for sympathetic neurons growing in co-culture with cardiomyocytes *in vitro* (micrographs were colored in post-processing). Scale bar: $25 \mu m$.

(B) Close up of a connection between neurite extension and cardiac syncytium showing connections between neurons and myocytes. Scale bar: $5 \mu m$.

(C–F) SEM images showing stellate sympathetic neurons on cardiac monolayers. Neurons making connections to other neurons (C), wide spreading neurite extensions (D), neuron bodies and extensions make contact with myocytes (E), white asterisk showing dendritic process (E) and white arrow (F) indicating neuron body. Scale bars: (C) 50, (D) 50, (E) 10, and (F) 20 μ m respectively.

See also Figure S1.

3] Wave Pattern Formation is Affected by the Presence of Neurons

Using off-axis dye-free imaging, we investigated how neuronal activation modulates cardiac patterns of activation in monolayer culture (Figure S5). Functional measurements were performed on the sample from day 5 onwards. We chose experimental conditions that spontaneously yield a wide variety of wavefront topologies within the imaging system's 16×16 mm field of view.

Introduction of an additional cell type can potentially introduce heterogeneities that would impact wave front stability. Surprisingly, co-cultures displayed fewer wave breaks than their monoculture counterparts





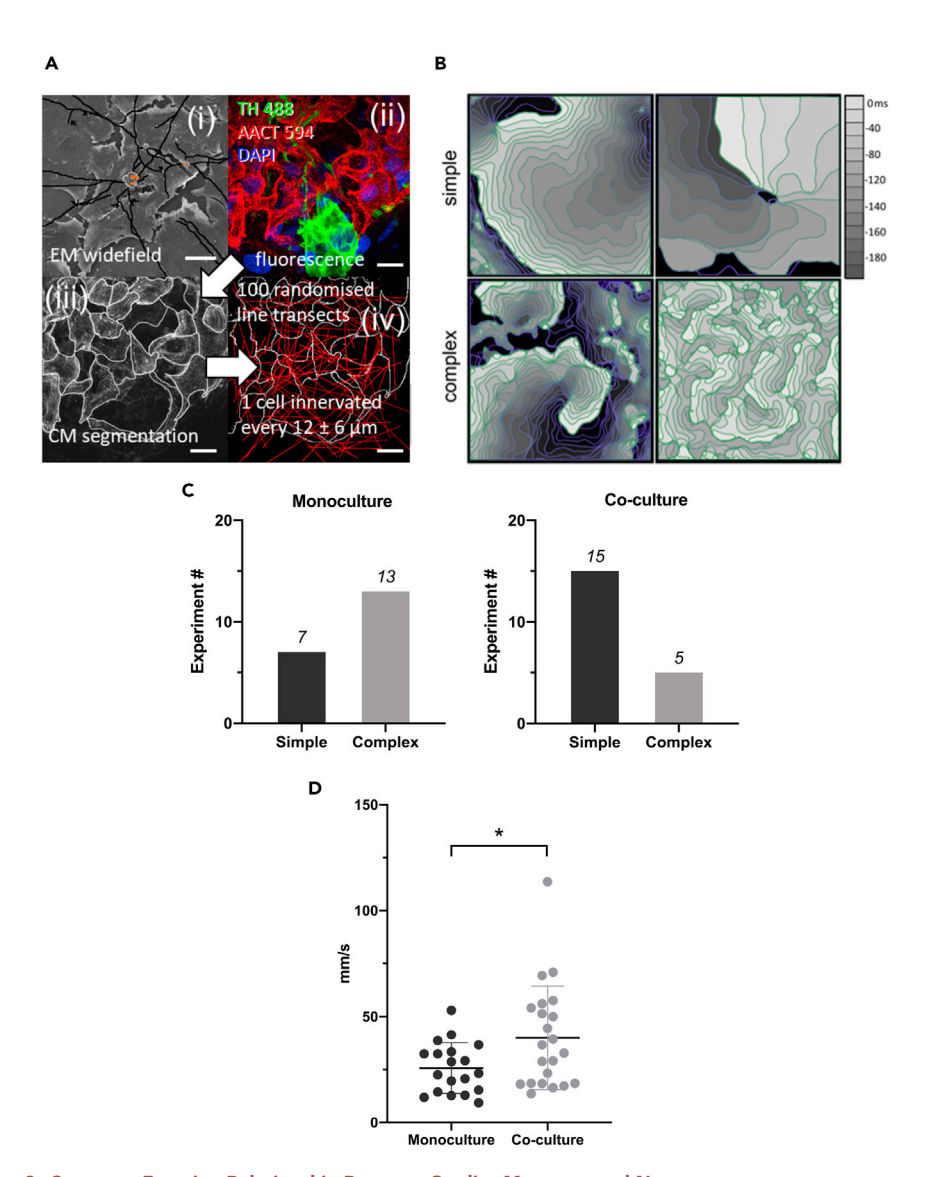


Figure 2. Structure-Function Relationship Between Cardiac Myocytes and Neurons

(A) (i) Wide-field scanning electron microscopy image of neuron cell bodies (square orange overlay) showing manual segmentation of dendritic processes traversing the CM monolayer (black lines). See Figure S1 for further images. (ii) Single slice from multichannel confocal stack of CM cells in monolayer (red) around a cell body (green) with nuclei (blue). (iii) Maximum intensity projection of CM channel from (iii) was manually segmented to highlight cell boundaries (white lines). (iv) Randomized linear trajectories were taken through the segmented image to identify the average distance between cell boundaries, indicating the total number of cells that can be innervated by a given length of dendritic process. Scale bars: (i) $50 \mu m$; (ii)–(iv) $20 \mu m$.

(B) Wave dynamics measured by dye-free imaging in Oxford monocultures and co-cultures (see also Figure S5). Isochronal maps of wave dynamics in confluent cardiac-stellate neuron co-cultures display a variety of complex rhythms similar to those seen in intact hearts. Wave dynamics here are classified as simple (top left: targets or top right: single spirals) or complex (bottom left: multiple spiral waves or bottom right: wavelets of activity).

(C) Monocultures display more complex dynamics than co-cultures, which display predominantly simple wavefronts with few wave breaks (p < 0.05, Chi-square).

(D) Comparison of 90-percentile of wave speed for monocultures (25.73 \pm 11.88 mm/s, n = 19) and co-cultures 39.96 \pm 24.37 (n = 22). Normal distribution of the data was confirmed using the Kolmogorov-Smirnov test, and data were compared using unpaired, two-tailed t-test (* indicates p = 0.026). Horizontal bars in D indicate data means \pm stdev. See Figure S13 for wave speeds in SBU cultures.

iScience Article



at similar plating densities (Figures 2B and 2C), i.e. neurons had stabilizing effect on cardiac wave dynamics. We broadly classified wave dynamics as simple [periodic target waves Figure 2B (top left) and single spiral wave reentry 2 B (top right)], or complex [single dominant spiral with additional irregular waves 2 B (bottom left) and multiple equally sized wavelets 2 B (bottom right)]. Although monocultures frequently displayed complex dynamics, co-cultures rarely displayed this behavior (Figure 2C, p < 0.05, chi-square test). Indeed, we observed wavelet reentry in only one of the co-culture preparations (6 isolations, 20 preparations, where the number of samples n = 20 tested here refers to individual petri dishes; these were obtained from at least 6 separate cell isolations).

4] Conduction Velocity in Spontaneously Active Oxford Co-cultures is Faster Than Myocyte Monocultures

We measured conduction velocity in unstimulated co-cultures (n = 22) and myocyte monocultures (n = 19). Figure 2D shows data representing the 90-percentile of wave speed from each recording. The conduction velocity in the co-cultures was significantly faster than in myocyte monocultures. Overall, the mean conduction velocity (\pm stdev) in the myocyte monocultures was 25.73 \pm 11.88 mm/s and 39.96 \pm 24.37 mm/s in the co-cultures. To try and understand the molecular mechanisms, we conducted quantitative label-free proteomics analysis on the myocyte and co-cultures (Tables S1 and S2, Figures S8 and S10). We found changes in pathways regulating gap junction protein expression along numerous changes in pathways associated with metabolism and development (Figures S8 and S10). Additional measurements of Connexin43 (Cx43) levels in cultures using western blot technique (Figure S12) confirmed that Cx43 was higher in the co-cultures (two independent experiments).

Interestingly, in better-connected Stony Brook University (SBU) co-cultures that were not spontaneously active/arrhythmic, the stimulated conduction velocities were very similar at 1 Hz electrical pacing for different neuron concentrations (Figure S13), showing no significant difference using ANOVA followed by Tukey-Kramer.

5a] Nicotine Stimulation Increases Beat Rate in Co-cultures Displaying Target Patterns

To confirm the formation of functional connections between cardiac myocytes and sympathetic stellate neurons (Figure 3 top panel), we stimulated the cardiac myocyte contraction rate through the activation of neurons with nicotine (n = 6), in a similar fashion to the way this was done in (Shcherbakova et al., 2007). In the co-cultures we observed an average increase in beat rate of 31% \pm 4 (standard error) when 10 μM of nicotine was added (up to 5 min post-nicotine addition and then the beat rate returned to baseline, Figure 3 bottom panel). We also performed (i) control experiments in which nicotine was added to cardiac monocultures (with no neurons present) and we did not see any changes in the contraction rate (p > 0.05); (ii) vehicle experiments in co-cultures (i.e. using distilled water equivalent to the quantity of nicotine used) show no increase in beat rate.

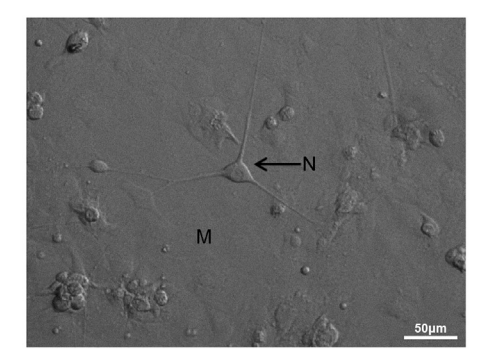
5b] Bath Application of Nicotine Produces a Marked Increase in Spontaneous Firing of Action Potentials in Co-cultured Neurons

Using the whole-cell current clamp method we observed repeated membrane depolarization events (in three separate experiments) on the addition of 10 μ M nicotine (Figure 4A). We measured the membrane potential of individual neurons within the co-culture at 0–60 s (pre) to 300–360 s (post) nicotine application and found a significant rise in membrane potential (p < 0.05, paired t -test). Figure S6 shows individual frames from a video recorded before and after nicotine application. The video was processed to show motion transients (white) as described in the supplement. Changes in cardiac macroscopic activity correlate with neuronal bursting following nicotine application.

6] One Neuron Potentially Stimulates a Connected Monolayer of One Hundred Thousand Myocytes

Pilot electrophysiology experiments (n = 3) suggested that a single neuron could potentially modulate the activity of many connected cardiomyocytes (Figure 4B). Current injection into a patched neuron caused a rapid activation of the neuron, which was correlated to irregular activity in the monolayer by calculating the cross-correlation between sequential frames in order to map changes. Electrophysiological measurement of neuron activity in co-cultures poses challenges such as trying to keep a patch on a neuron after





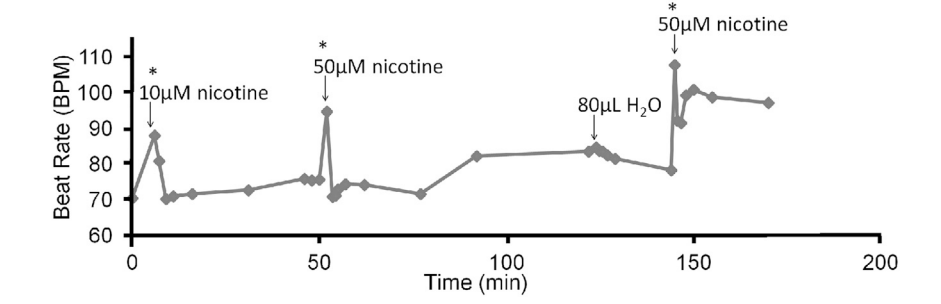


Figure 3. Cardiac Monolayer Response to Stellate Sympathetic Neuron Stimulation via Nicotine

(Top panel) Bright field image of a confluent cardiac monolayer with cardiac sympathetic stellate neurons seeded on top.

(Top panel) Bright field image of a confluent cardiac monolayer with cardiac sympathetic stellate neurons seeded on top. (Bottom panel) An example trace of a co-culture nicotine stimulation experiment. Each data point represents a 5-s video recording consisting of at least six full contractions. Repeat nicotine doses (10 and $50 \mu M$) caused transient increases in myocyte beat rate; control vehicle (distilled water) of the same volume had no effect. Comparisons between pre- and post-nicotine beat rates were performed using a t test; *p < 0.0001.

stimulating a "beating" cardiac monolayer. These observations formed the motivation for extensive optogenetic and optochemical-based experiments that follow.

7] Optogenetic and Optochemical Neuronal Stimulation and the Effect of Neurotransmitter Release on Cardiomyocytes Using High-Throughput Fluorescence Methods

Co-cultures were created by varying the neuron concentration cultured together on top of a monolayer of myocytes. Myocytes were plated in 96 well plates at plating density of 140,000 myocytes/well. The stellate sympathetic neurons were infected with hChR2-eYFP. Schematic representation of the co-cultures with different neuron dosing regimes (neuron-myocyte ratios in 1:5, 1:20, 1:100, 1:100,000) are shown in Figure 5A. Immunohistochemistry was used to confirm the presence of sympathetic neurons (using TH antibody) in the different neuron-myocyte co-culture ratio combinations (Figure S4). High-throughput fluorescence imaging methods (Klimas et al., 2020) of co-cultures also allowed the study of the effects of sympathetic cardiac stellate neurons on cardiac activity in well-connected quiescent cardiac cultures using optical mapping (cultures loaded with the near-infrared voltage-sensitive dye Di-4-ANBDQBS). Co-cultures were found to be constitutively more active than monocultures of myocytes (Figure S14) [Fishers exact test (two-sided), p = 0.0046 statistically significant, n = 6 myocytes and n = 24 for co-cultures].

Optogenetic neural stimulation of cardiac tissue via channelrhodopsin-2 (ChR2), selectively expressed only in the neurons, was performed using a light stimulation protocol schematically represented above plot 5 B(i) in Figure 5. Co-cultures of neurons and myocytes were loaded with dye Di-4-ANBDQBS, which is spectrally compatible with ChR2 (Klimas et al., 2020). Optical stimulation (470 nm) was provided at pulse lengths of 3 s, at 0.5 Hz, using irradiance of 0.5–1 mW/mm². Long light pulse stimulation results in action potentials evoked indirectly in the myocytes by ChR2-expressing neurons (Figures 5B(i) and S15E). Cardiac response to light stimulation of ChR2-expressing neurons shows a dose-dependent effect

iScience Article



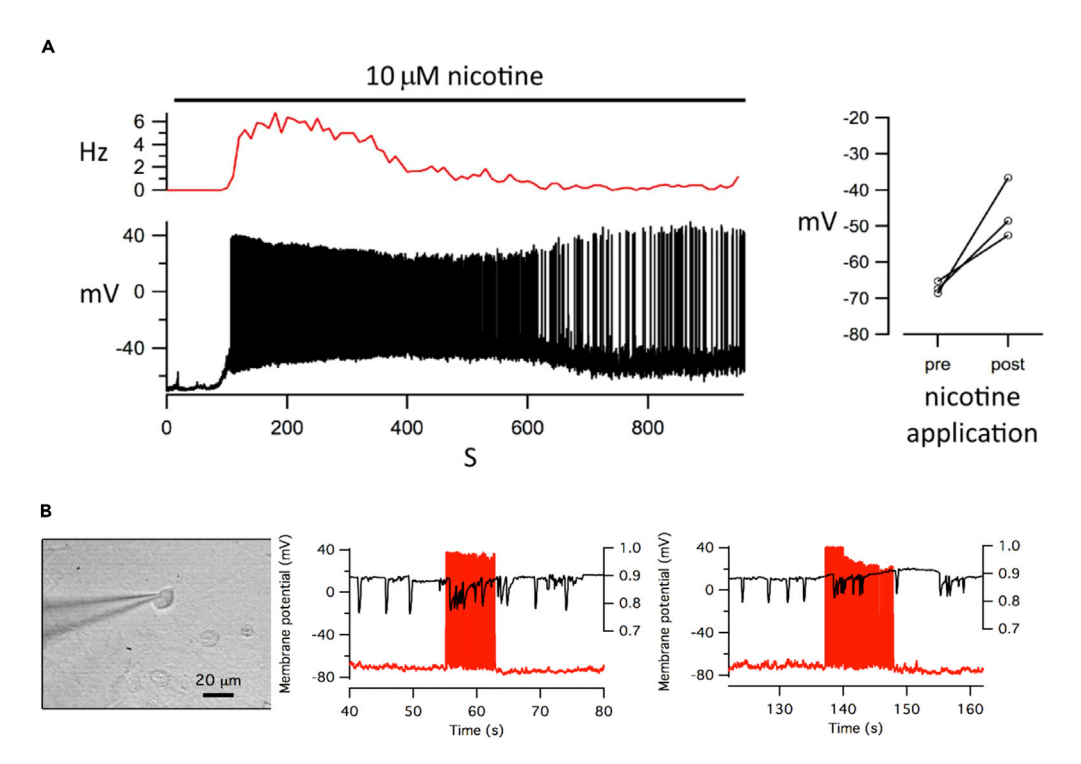


Figure 4. Simultaneous Electrophysiological Measurement of Neuron Membrane Potential and Video Imaging of Cardiac Dynamics

(A) The bath application of nicotine to co-cultures produced membrane depolarization and a marked increase in the spontaneous firing of action potential in a patched neuron. (p < 0.05, paired t test, n = 3). The side panel shows the net depolarization of the resting potential of neurons before and after nicotine application.

(B) Electrophysiological stimulation of one neuron can drive induced arrhythmia in co-cultures. Graphs show two examples in which injection of current into a patch-clamped neuron (red trace) changes cardiac behavior from normal beating to arrhythmia (black trace). Myocyte beat rate is shown by the downward deflections of the black trace, using frame cross-correlation of each video frame correlated to the original image in order to map changes. Synchronization of video imaging and electrophysiological trace is accurate to +/-2 s.

See also Figure S6.

(Figure 5B(ii)), where cultures with higher neuron concentrations generate more cardiac activity with the same light stimulus.

The normalized firing score is given as:

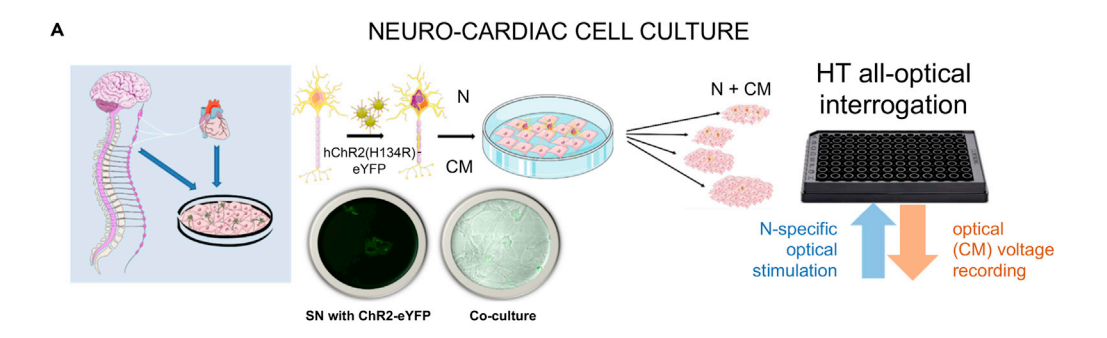
$$\frac{Ns}{Ps} - \frac{Nns}{Pns}$$
$$\frac{Ns}{Ps} + \frac{Nns}{Pns}$$

where Ns and Nns give the number of detected spikes during periods of stimulation and no stimulation, respectively. Ps and Pns give the fraction of the recording that is stimulated and not stimulated, respectively. This score lies between -1 (all spikes occurring during the nonstimulated period) and 1 (all spikes occurring during the stimulated period).

We also assessed the co-culture dynamics using an optochemical approach where caged nicotine was added to each well (Figure 5C), and nicotine is released with light stimulation (see also Figure S16). Although we observed cases where low-density co-cultures responded to nicotine uncaging (12/18 responders), either by increasing beat rate or by inducing bursting behavior in the cardiac monolayer, these responses occurred after a long delay, which raised the possibility that the effects may be due to chance. Longer recording times both pre- and post-light stimulation are required to confirm the efficacy of this method.







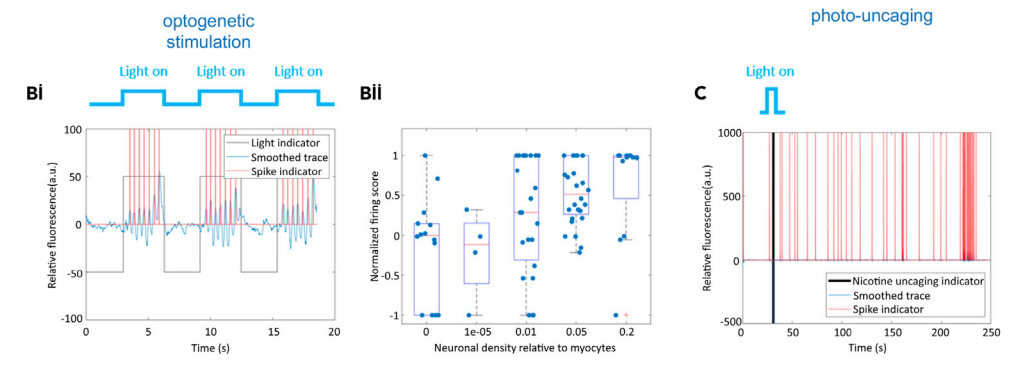


Figure 5. High Throughput All Optical Interrogation of Neurocardiac Cultures

(A) Schematic representation of the *in vitro* co-culture system, neonatal rat cardiac stellate sympathetic neurons, and neonatal rat ventricular cardiac confluent monolayers cultured to test sympathetic-cardiac interactions. The stellate sympathetic neurons were infected with hChR2-eYFP. Schematic representation of the co-cultures with different neuron dosing regimes (neuron-myocyte ratios in 1:5, 1:20, 1:100, 1:100,000).

(B and C) "Optoelectric" versus "optochemical" stimulation of neurons. (B) Optogenetic neural stimulation of cardiac tissue via Channelrhodopsin-2 (ChR2), selectively expressed only in the neurons. Co-cultures of neurons and myocytes (loaded with dye Di-4-ANBDQBS spectrally compatible with ChR2). Optical stimulation (470 nm) was provided at pulse lengths of 3 s, at 0.5 Hz, using irradiance of 0.5-1 mW/mm². (Bi) Post-processed traces using custom-written MATLAB software. Traces showing baseline no activity and followed by long light pulse stimulation, action potentials are evoked indirectly in the myocytes via the ChR2-light-sensitized neurons. Blue is the trace after baseline subtraction after median filtering, red indicates detected spike times, black is an indicator of when light is present (black down = light off). (Bii) The number of neurons innervating the myocytes affects the firing frequency of myocytes in cultures with different neuron to myocyte ratios (0 = myocytes/controls, 1 \times 10⁻⁵ = 1:100,000, 0.01 = 1:100, 0.05 = 1:20 and 0.2 = 1:5); the number of experiments (n) for each group were 14, 4, 23, 28, and 12 and confidence values (p) (against null hypothesis of zero effect; Wilcoxon signed rank test) were 0.7131, 0.6250, 0.1091, 0.0000, and 0.0352. We observe a dose-dependent effect (i.e. the greater the number of neurons innervating the myocytes, the greater the effect, with values greater than 0 indicating an increase in beat rate). (C) Photo-uncaging of nicotine using a flash of blue light may lead to the release of noradrenaline by the sympathetic neurons resulting in increase in myocyte beat rate. Panel A was created with Servier Medical Art according to a Creative Commons Attribution 3.0 Unported License guidelines 3.0. See also Figure S4 for immunohistochemistry; see also Figures S15-S17. SN: sympathetic neuron; N: neuron, CM: cardiomyocyte, HT: high throughput.

Standard (global) nicotine treatment of co-cultures to drive sympathetic neurons offers very little spatio-temporal control over the experiments (Figure S17). Optochemical methods to cause uncaging of nicotine to stimulate neurons, which in turn stimulate myocytes, can be achieved (Figures 5 C and S16). The timing of chemical release to stimulate neurons in culture to alter myocyte response (rate) can be controlled with some precision using this approach. At the same time, optogenetic stimulation of stellate sympathetic neurons offers far superior precise spatiotemporal control of neuron behavior and their effects on myocytes (Figures 5Bi and S15).

DISCUSSION

Emerging evidence supports the potential of neuromodulation therapy in clinical management and prevention of lethal arrhythmias (Meng et al., 2018), but direct neural-cardiac interactions (at the cell level)

iScience Article



are still understudied due to lack of specific tools with high spatiotemporal resolution. We demonstrate that interesting topics such as the effect of neural density on the electrophysiological properties of a cardiac syncytium can be studied at the multicellular level in a high-throughput manner using all-optical techniques. We report the rather unexpected finding that neuronal activation protects from developing activation wave breaks, regarded as an in vitro marker for arrhythmogenic behavior. Our work leveraged the use of dye-free mapping of activation wave fronts over a large field of view. Here we highlight (i) a methodology to study neuron-cardiac interactions at the multicellular/tissue level; (ii) findings on the relationship between neuron presence and macroscopic wave properties; (iii) and finally the relationship between neuron density in co-culture and cardiac firing rates. Photo-uncaging of nicotine or optogenetic neural stimulation are used here in conjunction with optical imaging of cardiomyocyte contractile and electrical activity to illustrate the power of such interrogations. We designed a simplified in vitro model of neurally modulated arrhythmogenesis by co-culturing stellate sympathetic neurons with confluent monolayers of myocytes and optically measured the effects of these neurons on cardiac wave speeds. We demonstrate that physical (Figure 1) and functional connections (Figures 2, 3, 4, and 5) are formed between cardiac sympathetic stellate nerve cells and cardiomyocytes as previously reported in isolated cell preparations (Himel et al., 2012; Prando et al., 2018; Tao et al., 2011).

Using optogenetic stimulation of catecholaminergic neurons (targeted via a TH-promoter) in transgenic mouse hearts, Wengrowski et al. (2015) showed immediate increase in heart rate and contractility. The basis of this interaction is the existence of specialized junctional sites between neurons and myocytes shown by Shcherbakova et al. (2007) and later Prando et al. (2018), who used coupled myocyte pairs to demonstrate that neurons raise intracellular cAMP only in directly contacted myocytes. In addition, there is a wealth of evidence that cardiac innervation is tightly linked to cardiac development and function. For example; nerve growth factor is required for sympathetic axon growth and innervation (leda et al., 2004; Kuruvilla et al., 2004; Lockhart et al., 2000) and SEMA3A expression is needed for sympathetic innervation patterning and appears to be critical for heart control (leda et al., 2007). Although these studies highlight the importance of local neuron myocyte connections, they raise questions related to how the density and distribution of these connections impact macroscopic wave propagation at the tissue level.

Microscopy studies have demonstrated that the density of cardiac innervation is normally very high (Freeman et al., 2014), with neuronal processes being close to almost every cardiomyocyte in intact myocardium. Neuron density can, however, dramatically change in response to disease states. For example, there is loss and gain of sympathetic axons in the border zone of a chronic myocardial infarction (Cao et al., 2000; Freeman et al., 2014; Zhou et al., 2004). The functional consequences of these variations remain unclear.

Although our experiments demonstrate that innervation results in functional changes in CV and changes the spatial organization of cardiac waves in vitro, the mechanisms responsible for these changes are unknown. Fibroblast concentration, gap junction density, and ion channel expression are known modulators of conduction velocity. Our immunofluorescence studies indicate low vimentin expression levels in the cultures, indicating low fibroblast proliferation (Figure S3); however, preliminary studies on gap junction protein Cx43 levels found that this protein was elevated in co-cultures relative to cardiac monocultures (Figure \$12). In addition, we performed a label-free quantitative proteomics analysis on cultures (see Tables S1, S2, S5, and S6); protein ratios (co-cultures/myocytes) were calculated from SINQ intensities (see Tables S5 and S6) for all quantified protein hits; and the regulation of randomly chosen proteins fibronectin and vimentin observed in proteomics were confirmed by western blots in 3 independent experiments (see Figure S11). We found changes in pathways regulating gap junction protein expression along with numerous changes in pathways associated with metabolism and development (Figures S8 and S10). The results of our proteomics screen is consistent with other studies that link innervation to developmental processes (Atkins et al., 1997; Larsen et al., 2016; Ogawa et al., 1992; Shcherbakova et al., 2007; Takeuchi et al., 2011). Shortly after birth, cardiomyocyte hyperplasia decreases and CV increases (Ogawa et al., 1992), along with increased β-adrenoreceptor density on cardiomyocytes and higher levels of catecholamines in the circulation (Claycomb, 1976). Recent studies (Kreipke and Birren, 2015) have demonstrated that having sympathetic neurons present in in-vitro cardiac cultures delays cardiomyocyte cell cycle withdrawal and transiently limits hypertrophy via a β-adrenergic signaling pathway, which suggests that sympathetic innervation can regulate cardiomyocyte numbers during the postnatal period. Developmental changes may occur in neurons as well: Oh et al. reported increased maturation of hiPSC-derived sympathetic neurons in their cardiac neuron co-culture system (Oh et al., 2016). Coppen et al. have suggested the existence





of post-natal changes in connexin expression in the developing fetal heart (Coppen et al., 2003). There is also additional evidence that expression of different connexin isotypes varies not only within distinct compartments of the adult heart but also as a function of cardiac developmental stage (Giovannone et al., 2012). It is possible that neurons enhance maturity of cardiomyocytes and the CV increase seen in our experiments may be due to developmental changes in the cardiac myocytes and improved connectivity.

Furthermore, our tissue culture results may also be relevant to understanding the effects of nerve sprouting in scar tissue and in helping to resolve the apparently conflicting results summarized in the Introduction. Our observation that co-cultures display fewer wave breaks than monocultures, have increased CV, and higher levels of Cx43 offer indirect support for the protective role of neurons in intact tissues, particularly in cases such as the infarct border zone, which shows reduced function of gap junctions and slower conduction (Luke and Saffitz, 1991). At the same time, the effects of acute nicotinic stimulation of neurons in our coculture system may be a model of proarrhythmogenicity in the hyperinnervated infarct border zone during a surge of the sympathetic drive.

Although conventional electrophysiology techniques allow for specific micro control of single cells or sparse cell cultures, the application of such techniques is technically challenging when studying two cell types grown in a syncytium (such as the spontaneously excitable cardiac tissue and neurons). Arthur Winfree (Winfree, 1987) hypothesized many years ago that the pattern of nervous system innervation could determine whether an arrhythmia could be instigated. Alterations in autonomic function occur in several interrelated cardiac conditions including sudden cardiac death, congestive heart failure, diabetic neuropathy, and myocardial ischemia (Vaseghi and Shivkumar, 2008). Neural modulation as a treatment for arrhythmias has been well established in certain diseases (such as long QT syndrome); however, in most other arrhythmias, it is still an open question and the subject of intense research (Herring et al., 2019). Ongoing research over the last five decades has highlighted the importance of communication between neural and cardiac tissues. The evidence that the role of excessive cardiac sympathetic activity can directly precipitate ventricular tachycardia has been provided by studies in patients and animal models with healed myocardial infarction (Billman, 2006; Janse et al., 1985; Jiang et al., 2008). However, the technical challenges of performing electrophysiological experiments motivated us to adopt an alternative, more "controlled" method to study the effects of neuron numbers on cardiac behavior, and these data are presented in Figure 5B where we opted for an optogenetic approach to control neurons and study the resulting cardiac behavior. We observe that increasing the number of neurons innervating the myocytes affects the firing frequency of myocytes in cultures. We report a dose-dependent effect (i.e. the greater the number of neurons innervating the myocytes, the greater the effect), where the highest effect on rate increase is observed in the 1:5 neuron-myocyte ratio cultures. Co-culture studies (Lockhart et al., 1997, 2000) focusing on myocyte maturation, nerve growth factor, and synapse formation between myocytes and sympathetic neurons have used similar physiological neuron-myocyte ratios (\sim 7500 neurons to \sim 75,000 myocytes).

In terms of neurocardiac interactions, Lockhart et al. (2000) put the average process length per neuron in co-culture to be 1.8 \pm 0.3 mm. We measured process length in SEM images and estimated the average process in our cultures to be 1,183 μm . Therefore, in 67% of cases each neuron will directly stimulate between 56 and 167 myocytes, with an average of 83 myocytes per neuron. This estimate is based on a two-dimensional model of neuron innervation and assumes that each point of contact between neuron and myocyte leads to a site of innervation.

The number of myocytes needed to initiate a wave of activity has been investigated using a variety of techniques and can be in the thousands in healthy, well connected tissue (Tveito and Lines, 2008; Xie et al., 2010; Zaglia et al., 2015). However, the minimum number of myocytes needed strongly depends on their connectivity, with simulations suggesting that this may be as low as 40 cells in poorly connected, fibrotic tissue. As the conduction velocity in our preparation (39 mm/s) is lower than those simulations (60 mm/s in fibrotic tissue simulations, Table 1 in Xie et al. (2010)), and since conduction velocity is a monotonic function of gap junction connectivity (Dhillon et al., 2013), these modeling studies provide a plausible mechanism for modulation of tissue level cardiac activity by a single neuron. The surprising neuron patch clamp pilot study result (Figure 4B) indicating that one neuron can potentially stimulate a connected monolayer of cardiac cells calls for further consideration for the role of neuron numbers and their potential impact during pathological conditions. We note in the experiments where 1:100,000 neuron/cardiomyocyte density was studied, the cardiac response to neuron stimulation was negligible; however, it is important to note

iScience Article



that at these densities some of the measured wells likely had zero neurons (see Transparent Methods, Section 4). From our experiments and previously published literature, it seems plausible that dendrites of one neuron can stimulate (through NA release) a big group of myocytes, which in turn then go on to stimulate their neighbors and consequently, the whole dish.

Although experimental challenges still need to be overcome, dissecting mechanisms along the heart-brain axis has become more achievable with the introduction of innovative methods, imaging (Bruegmann et al., 2010; Prando et al., 2018; Sigalas et al., 2020; Vaseghi et al., 2012), and tissue engineering techniques (Burton et al., 2015; Klimas et al., 2016). In summary, we investigated the effect of sympathetic innervation on the activation dynamics of a cardiac cell monolayer innervated in vitro by co-culture with stellate ganglia neurons. We report the rather unexpected finding that neuronal activation protects from developing activation wave breaks, regarded as an in vitro marker for arrhythmogenic behavior. Does the number of neurons innervating cardiac tissue matter? Our data suggest that the greater the number of neurons innervating the myocytes, the greater the cardiac effect observed. The utility and scope of our macroscopic co-culture model offers even greater potential. In addition to using dye-free approaches (Burton et al., 2015) to measure pattern formation and conduction velocity, all-optical electrophysiology allows for high-resolution, high-throughput fluorescent interrogation of neural influence on cardiac monolayers using optochemical and optogenetic stimulation (Figure 5) (Klimas et al., 2016), (Klimas et al., 2020). We have also extended this line of investigation from primary neonatal rat cells to human iPSC-derived peripheral neuron co-cultures as a proof of concept study (Axiogenesis [now Ncardia], Figure \$18). Thus, the methods described here provide approaches that could broaden our insight into fundamental human disease mechanisms. The use of in vitro techniques in pharmacological assays and profiling is growing in its popularity in the drug discovery process (Bowes et al., 2012). Our experimental model in conjunction with recently developed imaging platforms can be applied to improve the efficacy of preclinical drug toxicity and discovery studies. More structural and mechanistic knowledge on the sympathetic neuron numbers and patterns in the heart could offer a new step toward potential therapies for lethal arrhythmias.

Limitations of the Study

Although dye-free imaging offers long-term, non-contact precision control of wave properties that pharmacological and electrical methods lack, the interpretation of complex spiral wave patterns may be hindered by similarities in the optical signals from excitation and relaxation waves (Sigalas et al., 2020). Lowdensity neuron co-culture dishes offered interesting observations that may be of clinical relevance; however, the technical challenges of ensuring low numbers of neurons that are present and functional in these co-cultures currently highlight a limitation of this approach. Furthermore, the experiments in the present study did not control for organizational variations inherent within monolayer cultures. Although the techniques utilized here at the macroscopic level have clear advantages over the use of single-cells and monocultures, correlation of events observed at the neuron-cardiac junction in co-culture monolayers with in vivo activity will require further validation in intact tissue. In addition, current techniques for generating monolayer cultures rely on the harvesting of cardiomyocytes from neonatal animals. It is important to recognize that such neonatal cells exhibit a different morphology and phenotype compared with mature cells, further highlighting the requirement for in vivo validation at the level of the intact, mature heart. Future efforts can adapt these approaches to optimized human stem-cellderived cardiomyocyte tissue constructs and stem-cell-derived autonomic neurons for better relevance to human physiology.

Resource Availability

Lead Contact

Further information and requests for resources should be directed to and will be fulfilled by the Lead Contact, Rebecca Burton (Rebecca.burton@pharm.ox.ac.uk).

Materials Availability

This study did not generate new unique reagents.

Data and Code Availability

No new specialized code was used.





Proteomics Data: the mass spectrometry proteomics data have been deposited to the ProteomeXchange Consortium via the PRIDE (Perez-Riverol et al., 2019) partner repository with the dataset identifier PXD019908 and 10.6019/PXD019908.

The imaging datasets supporting the current study have not been deposited in a public repository because of the large nature of the files (\sim 1 Terabyte data) but are available from the corresponding author on request.

METHODS

All methods can be found in the accompanying Transparent Methods supplemental file.

SUPPLEMENTAL INFORMATION

Supplemental Information can be found online at https://doi.org/10.1016/j.isci.2020.101334.

ACKNOWLEDGMENTS

GB acknowledges salary support from Medical Research Council (United Kingdom) and the Canadian Heart and Stroke Foundation (Canada). RABB is funded by a Sir Henry Dale Wellcome Trust and Royal Society (United Kingdom) Fellowship (109371/Z/15/Z) and acknowledges support from The Returning Carers' Fund, Medical Sciences Division, University of Oxford (United Kingdom). EE was partially supported by NIH (United States) grant R01 HL144157-01A1 and NSF (United States) grants 1-623068, 1705645, 1830941, 1827535. RABB is a Winston Churchill Fellow and received some travel support from the Winston Churchill Trust (United Kingdom) for part of this study. RABB is a Senior Research Fellow of at Linacre College, Oxford (United Kingdom). RAC is a post-doctoral scientist funded by the Wellcome Trust and Royal Society. JT acknowledges support from the EPSRC (United Kingdom) and Bakala Foundation (Czech). NH is a British Heart Foundation (BHF) Intermediate Fellow (FS/15/8/3115). SJB is funded by a British Heart Foundation (United Kingdom) Project Grant (PG/18/4/33521).

This study was funded by the BHF Centre of Research Excellence, Oxford, United Kingdom RE/18/3/34214 (GB, NH, DJP) and the EPSRC (Developing Leaders Grant held by RABB) and the Wellcome Trust and Royal Society (RABB). This study was also supported by a BHF project grant (PG/11/6/28660) to DJP and NH.

We would like to thank Dr Claudia Juarez Molina, Dr Suhail Aslam, and Bevin Gangadharan for technical help. We also thank Prof Gary Mirams from the University of Nottingham for commenting on parts of the statistics and Dr's Winbo and Montgomery for general scientific discussions that were supported by the Colin Pillinger International Exchanges Award. We thank Prof Helen Christian for valuable advice on the segmentation of the SEM images. We also thank Prof Kevin Webb, University of Nottingham for help with color segmentation of Figure 1A.

AUTHOR CONTRIBUTIONS

RABB performed tissue culture experiments. RABB and GB carried out all imaging experiments and played a major role in the writing of the paper. JT performed data analysis. CMA, A Klimas, and RABB set up and carried out high-throughput fluorescent (OptoDyCE) experiments in Stony Brook, USA. HEL, ARS, and EM performed patch clamp experiments on neurons. RAC performed Western blots. SB, GS, and DL contributed to setting up the initial co-culture experiments. RABB, HL, GG, and HK performed proteomics and analysis. A Kumar performed mass spectrometry. RABB, EE, and GB were responsible for experimental design. ADC and MC performed confocal and SEM cardiac and neuron image measurements and analysis. SJB contributed to running statistics (Figure 2), commenting on the draft and figures. All experiments were carried out in the laboratories of GB, DJP, and EE. All authors contributed to the writing and editing of the manuscript.

DECLARATION OF INTERESTS

The authors declare no competing interests.

iScience

Article



Received: September 19, 2019

Revised: May 12, 2020 Accepted: June 26, 2020 Published: July 24, 2020

REFERENCES

Atkins, D.L., Krumm, P.A., Schutte, B.C., Harrison, J.D., and Green, S.H. (1997). Regulation of rat cardiac myocyte growth by a neuronal factor secreted by PC12 cells. Pediatr. Res. 41, 832–841.

Bers, D.M. (2008). Calcium cycling and signaling in cardiac myocytes. Annu. Rev. Physiol. *70*, 23–49.

Billman, G.E. (2006). Heart rate response to onset of exercise: evidence for enhanced cardiac sympathetic activity in animals susceptible to ventricular fibrillation. Am. J. Physiol. Heart Circ. Physiol. 291, H429–H435.

Boogers, M.J., Borleffs, C.J., Henneman, M.M., van Bommel, R.J., van Ramshorst, J., Boersma, E., Dibbets-Schneider, P., Stokkel, M.P., van der Wall, E.E., Schalij, M.J., et al. (2010). Cardiac sympathetic denervation assessed with 123-iodine metaiodobenzylguanidine imaging predicts ventricular arrhythmias in implantable cardioverter-defibrillator patients. J. Am. Coll. Cardiol. 55, 2769–2777.

Bowes, J., Brown, A.J., Hamon, J., Jarolimek, W., Sridhar, A., Waldron, G., and Whitebread, S. (2012). Reducing safety-related drug attrition: the use of in vitro pharmacological profiling. Nat. Rev. Drug Discov. 11, 909–922.

Bruegmann, T., Malan, D., Hesse, M., Beiert, T., Fuegemann, C.J., Fleischmann, B.K., and Sasse, P. (2010). Optogenetic control of heart muscle in vitro and in vivo. Nat. Methods 7, 897–U845.

Bub, G., and Burton, R.A. (2014). Macro-micro imaging of cardiac-neural circuits in co-cultures from normal and diseased hearts. J. Physiol. 2014, 14

Burton, R.A., Klimas, A., Ambrosi, C.M., Tomek, J., Corbett, A., Entcheva, E., and Bub, G. (2015). Optical control of excitation waves in cardiac tissue. Nat. Photon. *9*, 813–816.

Cao, J.M., Fishbein, M.C., Han, J.B., Lai, W.W., Lai, A.C., Wu, T.J., Czer, L., Wolf, P.L., Denton, T.A., Shintaku, I.P., et al. (2000). Relationship between regional cardiac hyperinnervation and ventricular arrhythmia. Circulation 101, 1960–1969.

Chen, P.S., Chen, L.S., Cao, J.M., Sharifi, B., Karagueuzian, H.S., and Fishbein, M.C. (2001). Sympathetic nerve sprouting, electrical remodeling and the mechanisms of sudden cardiac death. Cardiovasc. Res. 50, 409–416.

Chen, P.S., Chen, L.S., Fishbein, M.C., Lin, S.F., and Nattel, S. (2014). Role of the autonomic nervous system in atrial fibrillation: pathophysiology and therapy. Circ. Res. *114*, 1500–1515.

Clarke, G.L., Bhattacherjee, A., Tague, S.E., Hasan, W., and Smith, P.G. (2010). ssadrenoceptor blockers increase cardiac sympathetic innervation by inhibiting autoreceptor suppression of axon growth. J. Neurosci. *30*, 12446–12454.

Claycomb, W.C. (1976). Biochemical aspects of cardiac muscle differentiation. Possible control of deoxyribonucleic acid synthesis and cell differentiation by adrenergic innervation and cyclic adenosine 3':5'-monophosphate. J. Biol. Chem. 251, 6082–6089.

Cohn, J.N., Levine, T.B., Olivari, M.T., Garberg, V., Lura, D., Francis, G.S., Simon, A.B., and Rector, T. (1984). Plasma norepinephrine as a guide to prognosis in patients with chronic congestive heart failure. N. Engl. J. Med. 311, 819–823.

Coppen, S.R., Kaba, R.A., Halliday, D., Dupont, E., Skepper, J.N., Elneil, S., and Severs, N.J. (2003). Comparison of connexin expression patterns in the developing mouse heart and human foetal heart. Mol. Cell. Biochem. 242, 121–127.

Devinsky, O. (2004). Effects of seizures on autonomic and cardiovascular function. Epilepsy Curr. 4, 43–46.

Dhillon, P.S., Gray, R., Kojodjojo, P., Jabr, R., Chowdhury, R., Fry, C.H., and Peters, N.S. (2013). Relationship between gap-junctional conductance and conduction velocity in mammalian myocardium. Circ. Arrhythm. Electrophysiol. *6*, 1208–1214.

Entcheva, E., and Bien, H. (2006). Macroscopic optical mapping of excitation in cardiac cell networks with ultra-high spatiotemporal resolution. Prog. Biophys. Mol. Biol. 92, 232–257.

Fallavollita, J.A., Heavey, B.M., Luisi, A.J., Jr., Michalek, S.M., Baldwa, S., Mashtare, T.L., Jr., Hutson, A.D., Dekemp, R.A., Haka, M.S., Sajjad, M., et al. (2014). Regional myocardial sympathetic denervation predicts the risk of sudden cardiac arrest in ischemic cardiomyopathy. J. Am. Coll. Cardiol. 63, 141–149.

Fallavollita, J.A., Dare, J.D., Carter, R.L., Baldwa, S., and Canty, J.M., Jr. (2017). Denervated myocardium is preferentially associated with sudden cardiac arrest in ischemic cardiomyopathy: a pilot competing risks analysis of cause-specific mortality. Circ. Cardiovasc. Imaging 10, e006446.

Freeman, K., Tao, W., Sun, H., Soonpaa, M.H., and Rubart, M. (2014). In situ three-dimensional reconstruction of mouse heart sympathetic innervation by two-photon excitation fluorescence imaging. J. Neurosci. Methods 221, 48–61

Furshpan, E.J., MacLeish, P.R., O'Lague, P.H., and Potter, D.D. (1976). Chemical transmission between rat sympathetic neurons and cardiac myocytes developing in microcultures: evidence for cholinergic, adrenergic, and dual-function neurons. Proc. Natl. Acad. Sci. U S A 73, 4225–4229.

Gardner, R.T., Wang, L., Lang, B.T., Cregg, J.M., Dunbar, C.L., Woodward, W.R., Silver, J., Ripplinger, C.M., and Habecker, B.A. (2015). Targeting protein tyrosine phosphatase sigma after myocardial infarction restores cardiac sympathetic innervation and prevents arrhythmias. Nat. Commun. 6, 6235.

Gardner, R.T., Ripplinger, C.M., Myles, R.C., and Habecker, B.A. (2016). Molecular mechanisms of sympathetic remodeling and arrhythmias. Circ. Arrhythm. Electrophysiol. *9*, e001359.

Giovannone, S., Remo, B.F., and Fishman, G.I. (2012). Channeling diversity: gap junction expression in the heart. Heart Rhythm 9, 1159–1162.

Herring, N., Kalla, M., and Paterson, D.J. (2019). The autonomic nervous system and cardiac arrhythmias: current concepts and emerging therapies. Nat. Rev. Cardiol. *16*, 707–726.

Himel, H.D.I.V., Bub, G., Lakireddy, P., and El-Sherif, N. (2012). Optical imaging of arrhythmias in the cardiomyocyte monolayer. Heart Rhythm *9*, 2077–2082.

Horackova, M., Huang, M.H., Armour, J.A., Hopkins, D.A., and Mapplebeck, C. (1993). Cocultures of adult ventricular myocytes with stellate ganglia or intrinsic cardiac neurones from Guinea pigs: spontaneous activity and pharmacological properties. Cardiovasc. Res. 27, 1101–1108

leda, M., Fukuda, K., Hisaka, Y., Kimura, K., Kawaguchi, H., Fujita, J., Shimoda, K., Takeshita, E., Okano, H., Kurihara, Y., et al. (2004). Endothelin-1 regulates cardiac sympathetic innervation in the rodent heart by controlling nerve growth factor expression. J. Clin. Invest. 113, 876–884.

leda, M., Kanazawa, H., Kimura, K., Hattori, F., leda, Y., Taniguchi, M., Lee, J.K., Matsumura, K., Tomita, Y., Miyoshi, S., et al. (2007). Sema3a maintains normal heart rhythm through sympathetic innervation patterning. Nat. Med. 13, 604–612.

Janse, M.J., Schwartz, P.J., Wilms-Schopman, F., Peters, R.J., and Durrer, D. (1985). Effects of unilateral stellate ganglion stimulation and ablation on electrophysiologic changes induced by acute myocardial ischemia in dogs. Circulation 72, 585–595.

Jiang, H., Hu, X., Lu, Z., Wen, H., Zhao, D., Tang, Q., and Yang, B. (2008). Effects of sympathetic nerve stimulation on ischemia-induced ventricular arrhythmias by modulating connexin43 in rats. Arch. Med. Res. *39*, 647–654.

Julius, S. (1998). Effect of sympathetic overactivity on cardiovascular prognosis in hypertension. Eur. Heart J. 19, F14–F18.



iScience Article

Kleber, A.G., and Rudy, Y. (2004). Basic mechanisms of cardiac impulse propagation and associated arrhythmias. Physiol. Rev. 84, 431–488.

Klimas, A., Ambrosi, C.M., Yu, J., Williams, J.C., Bien, H., and Entcheva, E. (2016). OptoDyCE as an automated system for high-throughput alloptical dynamic cardiac electrophysiology. Nat. Commun. 7, 11542.

Klimas, A., Ortiz, G., Boggess, S.C., Miller, E.W., and Entcheva, E. (2020). Multimodal on-axis platform for all-optical electrophysiology with near-infrared probes in human stem-cell-derived cardiomyocytes. Prog. Biophys. Mol. Biol. 154, 62–70

Kreipke, R.E., and Birren, S.J. (2015). Innervating sympathetic neurons regulate heart size and the timing of cardiomyocyte cell cycle withdrawal. J. Physiol. *593*, 5057–5073.

Kuruvilla, R., Zweifel, L.S., Glebova, N.O., Lonze, B.E., Valdez, G., Ye, H., and Ginty, D.D. (2004). A neurotrophin signaling cascade coordinates sympathetic neuron development through differential control of TrkA trafficking and retrograde signaling. Cell *118*, 243–255.

Larsen, H.E., Lefkimmiatis, K., and Paterson, D.J. (2016). Sympathetic neurons are a powerful driver of myocyte function in cardiovascular disease. Sci. Rep. 6, 38898.

Lockhart, S.T., Mead, J.N., Pisano, J.M., Slonimsky, J.D., and Birren, S.J. (2000). Nerve growth factor collaborates with myocyte-derived factors to promote development of presynaptic sites in cultured sympathetic neurons. J. Neurobiol. 42, 460–476.

Lockhart, S.T., Turrigiano, G.G., and Birren, S.J. (1997). Nerve growth factor modulates synaptic transmission between sympathetic neurons and cardiac myocytes. J. Neurosci. 17, 9573–9582.

Luke, R.A., and Saffitz, J.E. (1991). Remodeling of ventricular conduction pathways in healed canine infarct border zones. J. Clin. Invest. 87, 1594–1602.

Meng, L., Shivkumar, K., and Ajijola, O. (2018). Autonomic regulation and ventricular arrhythmias. Curr. Treat. Options Cardiovasc. Med. 20, 38.

Muhlfeld, C., Papadakis, T., Krasteva, G., Nyengaard, J.R., Hahn, U., and Kummer, W. (2010). An unbiased stereological method for efficiently quantifying the innervation of the heart and other organs based on total length estimations. J. Appl. Physiol. (1985) 108, 1402– 1409.

Nishisato, K., Hashimoto, A., Nakata, T., Doi, T., Yamamoto, H., Nagahara, D., Shimoshige, S., Yuda, S., Tsuchihashi, K., and Shimamoto, K. (2010). Impaired cardiac sympathetic innervation and myocardial perfusion are related to lethal arrhythmia: quantification of cardiac tracers in patients with ICDs. J. Nucl. Med. 51, 1241–1249.

Ogawa, S., Barnett, J.V., Sen, L., Galper, J.B., Smith, T.W., and Marsh, J.D. (1992). Direct contact between sympathetic neurons and rat cardiac myocytes in vitro increases expression of functional calcium channels. J. Clin. Invest. 89, 1085–1093.

Oh, Y., Cho, G.S., Li, Z., Hong, I., Zhu, R., Kim, M.J., Kim, Y.J., Tampakakis, E., Tung, L., Huganir, R., et al. (2016). Functional coupling with cardiac muscle promotes maturation of hPSC-derived sympathetic neurons. Cell Stem Cell *19*, 95–106.

Perez-Riverol, Y., Csordas, A., Bai, J., Bernal-Llinares, M., Hewapathirana, S., Kundu, D.J., Inuganti, A., Griss, J., Mayer, G., Eisenacher, M., et al. (2019). The PRIDE database and related tools and resources in 2019: improving support for quantification data. Nucleic Acids Res. 47, D442–D450.

Prando, V., Da Broi, F., Franzoso, M., Plazzo, A.P., Pianca, N., Francolini, M., Basso, C., Kay, M.W., Zaglia, T., and Mongillo, M. (2018). Dynamics of neuroeffector coupling at cardiac sympathetic synapses. J. Physiol. 596, 2055–2075.

Shaw, R.M., and Rudy, Y. (1997). Ionic mechanisms of propagation in cardiac tissue. Roles of the sodium and L-type calcium currents during reduced excitability and decreased gap junction coupling. Circ. Res. 81, 727–741.

Shcherbakova, O.G., Hurt, C.M., Xiang, Y., Dell'Acqua, M.L., Zhang, Q., Tsien, R.W., and Kobilka, B.K. (2007). Organization of β -adrenoceptor signaling compartments by sympathetic innervation of cardiac myocytes. J. Cell Biol. *176*, 521–533.

Sigalas, C., Cremer, M., Winbo, A., Bose, S.J., Ashton, J.L., Bub, G., Montgomery, J.M., and Burton, R.A. (2020). Combining tissue engineering and optical imaging approaches to explore interactions along the neuro-cardiac axis. R. Soc. Open Sci. 7, 200265.

Standen, N.B., Quayle, J.M., Davies, N.W., Brayden, J.E., Huang, Y., and Nelson, M.T. (1989). Hyperpolarizing vasodilators activate ATP-sensitive K+ channels in arterial smooth muscle. Science 245, 177–180.

Takeuchi, A., Nakafutami, S., Tani, H., Mori, M., Takayama, Y., Moriguchi, H., Kotani, K., Miwa, K., Lee, J.K., Noshiro, M., et al. (2011). Device for co-culture of sympathetic neurons and cardiomyocytes using microfabrication. Lab Chip 11, 2268–2275.

Tao, T., Paterson, D.J., and Smith, N.P. (2011). A model of cellular cardiac-neural coupling that captures the sympathetic control of sinoatrial node excitability in normotensive and hypertensive rats. Biophys. J. 101, 594–602.

Tomek, J., Hao, G., Tomková, M., Lewis, A., Carr, C., Paterson, D.J., Rodriguez, B., Bub, G., and Herring, N. (2019). B-Adrenergic receptor stimulation and alternans in the border zone of a healed infarct: an ex vivo study and computational investigation of arrhythmogenesis. Front. Physiol. 10, 350.

Tomek, J., Rodriguez, B., Bub, G., and Heijman, J. (2017). β-Adrenergic receptor stimulation inhibits proarrhythmic alternans in postinfarction border zone cardiomyocytes: a computational analysis. Am. J. Physiol. Heart Circ. Physiol. 313, H338–H353

Tung, L., and Zhang, Y. (2006). Optical imaging of arrhythmias in tissue culture. J. Electrocardiol. *39*, S2–S6.

Tveito, A., and Lines, G.T. (2008). A condition for setting off ectopic waves in computational models of excitable cells. Math. Biosci. *213*, 141–150.

Vaseghi, M., Lux, R.L., Mahajan, A., and Shivkumar, K. (2012). Sympathetic stimulation increases dispersion of repolarization in humans with myocardial infarction. Am. J. Physiol. Heart Circ. Physiol. 302, H1838–H1846.

Vaseghi, M., and Shivkumar, K. (2008). The role of the autonomic nervous system in sudden cardiac death. Prog. Cardiovasc. Dis. 50, 404–419.

Wengrowski, A.M., Wang, X., Tapa, S., Posnack, N.G., Mendelowitz, D., and Kay, M.W. (2015). Optogenetic release of norepinephrine from cardiac sympathetic neurons alters mechanical and electrical function. Cardiovasc. Res. *105*, 143–150.

Winfree, A.T. (1987). When Time Breaks Down: The Three-Dimensional Dynamics of Electrochemical Waves and Cardiac Arrhythmias (Princeton University Press).

Xie, Y., Sato, D., Garfinkel, A., Qu, Z., and Weiss, J.N. (2010). So little source, so much sink: requirements for afterdepolarizations to propagate in tissue. Biophys. J. 99, 1408–1415.

Zaccolo, M., and Pozzan, T. (2002). Discrete microdomains with high concentration of cAMP in stimulated rat neonatal cardiac myocytes. Science *295*, 1711–1715.

Zaglia, T., Pianca, N., Borile, G., Da Broi, F., Richter, C., Campione, M., Lehnart, S.E., Luther, S., Corrado, D., Miquerol, L., et al. (2015). Optogenetic determination of the myocardial requirements for extrasystoles by cell typespecific targeting of ChannelRhodopsin-2. Proc. Natl. Acad. Sci. U S A 112, E4495–E4504.

Zhou, S., Chen, L.S., Miyauchi, Y., Miyauchi, M., Kar, S., Kangavari, S., Fishbein, M.C., Sharifi, B., and Chen, P.S. (2004). Mechanisms of cardiac nerve sprouting after myocardial infarction in dogs. Circ. Res. 95, 76–83.

Supplemental Information

Optical Interrogation of Sympathetic

Neuronal Effects on Macroscopic

Cardiomyocyte Network Dynamics

Rebecca-Ann B. Burton, Jakub Tomek, Christina M. Ambrosi, Hege E. Larsen, Amy R. Sharkey, Rebecca A. Capel, Alexander D. Corbett, Samuel Bilton, Aleksandra Klimas, Guy Stephens, Maegan Cremer, Samuel J. Bose, Dan Li, Giuseppe Gallone, Neil Herring, Edward O. Mann, Abhinav Kumar, Holger Kramer, Emilia Entcheva, David J. Paterson, and Gil Bub

TRANSPARENT METHODS:

All UK experiments were performed in accordance to UK Home Office Animals Scientific Procedures Act (1986). All experiments performed in the US were per an approved Stony Brook University IACUC protocol.

1] Cell Cultures:

a) Spontaneously active cell culture (Oxford culture): Here we use a neonatal ventricular cardiac monolayer cell culture model that spontaneously displays a wide range of behaviors (Burton et al., 2015) to investigate how neurons modulate pacemaking and reentrant activity. We measured activity (i) using a macroscopic dye free optical mapping imaging modality, (ii) patch clamp electrophysiology coupled with video microscopy and (iii) microscopic optical mapping. Hearts were isolated from neonatal SD rat pups (P1-P3), killed by Schedule 1 in accordance to UK Home Office Animals Scientific Procedures Act (1986). Ventricular myocytes were enzymatically isolated by a series of enzymatic digestions in trypsin (1mg/mL, Sigma Aldrich, UK) followed by collagenase (1mg/mL, Sigma Aldrich, UK) and triturated to achieve a suspension of cardiomyocytes. The isolated cells were then pre-plated in an incubator (37°C, 5% CO2) for an hour to allow most fibroblasts to settle at the bottom of the dish. The ventricular myocytes in the supernatant were then carefully removed from the dish and a cell count performed using a haemocytometer and trypan blue. The myocytes were plated on 35 mm poly-lysine coated petri-dishes (Bio coat Poly-D-Lysine 35mm petriplates, Corning, UK) at a density of 750,000 cells (per 35 mm petri-dish) in plating medium (85% DMEM, 17% M199, 10% Horse serum, 5% FBS and 1% penicillin/streptomycin, all from Sigma Aldrich). 24 hours later the cardiac sympathetic stellate neurons were isolated from litter mates as described previously with some modifications (He and Baas, 2003, Li et al., 2012). Briefly, following microscopic dissection of the sympathetic stellate ganglia, enzymatic digestion in trypsin 1mg/mL (Worthington, USA) and collagenase type-4 1 mg/mL (Worthington, USA), cells were dissociated by sequential mechanical trituration using fine (fire-polished) glass pipettes. Neurons were pre-plated for 1 hour (to eliminate fibroblast and Schwann cells), counted and plated in at varying neuron to myocyte ratios. Cocultures were created by plating neurons on top of the cardiac monolayers. Co-cultures were maintained in media supplemented with nerve growth factor (50 ng/mL, NGF Millipore), which promotes neuron development. The same high serum level media (maintaining the original serum concentrations of 10% horse serum and 5% FBS), was refreshed every other day, which supports the spontaneously active cardiac monolayers. The pre-plating steps and serum levels differ from the SBU cultures described in 1(b), which are the key differentiating steps and between these cultures that are spontaneously active.

Stimulation of cardiac sympathetic stellate neurons with nicotine: To measure the effects of neuron stimulation on myocyte beat rate, 10 μM nicotine ([-] nicotine hydrogen tartrate salt; Sigma-Aldrich) was used. Washout was performed with pre-warmed media.

b) Neonatal rat ventricular cardiomyocyte Culture (Stony Brook University culture-SBU): Neonatal (2–3-day old) Sprague—Dawley rats were killed by Schedule 1 and ventricular tissue was removed as per an approved Stony Brook University IACUC protocol (New York, USA). The ventricular tissue was digested in trypsin made up in in Hanks' Balanced Salt Solution (1 mg/mL, US Biochemical, Cleveland, OH) overnight at 4°C. The tissue was serially digested using 1 mg/mL collagenase (Worthington Biomedical, Lakewood, NJ) in HBSS at 37 °C and pipetted into conical tubes and placed on ice. After centrifugation, cells were re-suspended in culture medium M199 (GIBCO) supplemented

with 12 μM L-glutamine (GIBCO), 0.05 μg/mL penicillin-streptomycin (Mediatech Cellgro, Kansas City, MO), 0.2 μg/mL vitamin B12 (Sigma-Aldrich, St. Louis, MO), 10 mM HEPES (GIBCO), 3.5 mg/mL D-(+)-glucose (Sigma-Aldrich) and 10% fetal bovine serum, FBS (GIBCO). Fibroblasts were removed via a two-step pre-plating process, where the cell suspension was plated in a flask and incubated (37 °C, 5% CO2) for 45–60 min and switched to a new flask and the incubation repeated. Cardiomyocytes were then counted using a hemocytometer before plating in glass-bottom 96-well plates (*In Vitro* Scientific). 24 hours later the cardiac sympathetic stellate neurons were isolated from litter mates and co-cultured with the cardiomyocytes as described above in Cell Culture Methods. Low serum (2%) maintenance media was used from day 2.

96 well microscopic optical recording of SBU co-cultures with voltage-sensitive dye using high throughput fluorescent methods: Isolated neonatal cardiac cells were plated on fibronectin coated 96-well glass-bottom plates (In Vitro Scientific, P96-1-N). After 24 hours, stellate ganglia were isolated from litter mate pups (P3) and neurons isolated as described above, and plated on top of the myocytes. We performed optical recording of membrane voltage using the voltage-sensitive dye Di-4-ANBDQBS (from Leslie Loew, University of Connecticut), in normal Tyrode solution (4-5 days after cell plating). We compared a high dose versus low dose myocyte neuron co-culture combination (i.e. 1:5 (1 neuron stimulating 5 myocytes) and 1:100,000 (1 neuron stimulating 100,000 myocytes)) to determine the effect of neuron density on myocyte activity. Neurons were stimulated using 100 µM caged nicotine (RuBi-Nicotine, Cat No. 3855, Tocris). Measurements were carried out at room temperature as the multi-well plate setup did not accommodate a stage top incubator. We only analysed data from wells where the tissue was quiescent or beating with a rate lower than 1 Hz before nicotine stimulation: in particular recordings from monolayers that displayed bursting dynamics before nicotine stimulation were not used. Three of the wells displayed bursting dynamics before nicotine stimulation and were excluded from subsequent analysis.

Drugs: Stimulation of cardiac sympathetic stellate neurons with nicotine: To measure the effects of neuron stimulation on myocyte beat rate, 10 μM nicotine ([–] nicotine hydrogen tartrate salt; Sigma-Aldrich) was used. Washout was performed with pre-warmed media. In case of caged nicotine experiments, caged nicotine known as RuBiNic (RuBi-Nicotine, Cat No. 3855, Tocris) has been used in neurotransmission studies (Filevich *et al.*, 2010b). Uncaging can be extremely rapid, controlled in time or space and quantitatively controlled and repeated. We tested the following neuron-myocyte densities: 1:5, 1:20 and 1:100. We employed caged nicotine at 100 μM as the actual amount of uncaged drug is usually extremely small based on details in (Macgregor *et al.*, 2007).

2] Dye-free measurement of wave dynamics (Oxford dye-free macroscopic imaging): Our experimental goal was to determine how the addition of neurons modulates activation patterns in cardiac culture under a wide range of initial conditions. We found that cultures plated on poly-D-lysine coated plastic petri dishes and continuously maintained high serum conditions (10% Horse serum, 5% FBS) resulted in isotropic cultures that spontaneously display a wide range of excitation patterns (called here Oxford cultures).

Experimental conditions between research groups differ, but typically cultures by other groups are prepared by plating tissue on fibronectin coated glass coverslips, use low serum conditions after two days in culture, and perform imaging experiments after transferring dishes to a chamber in standard Tyrode solution in normal atmosphere. However, in our

hands cultures prepared in these conditions often require pacing to induce activity, which was not compatible with our experimental aim of finding how the addition of neurons modulate spontaneous cardiac activity.

We used dye-free imaging techniques (Hwang *et al.*, 2005) with modifications as described in (Burton *et al.*, 2015) to image the spontaneously active confluent monolayers (Oxford cultures). Here, we employed an Olympus MVX10 Macroscope and Andor Neo sCMOS camera to record wave patterns and beat rate (from day 3 onwards). Experiments were carried out in an Okolab (Indigo Scientific, UK) stage incubation chamber controlled for heat (32 - 37°C), CO2 (5%) and humidity. Culture plates were allowed to equilibrate in these conditions for 20 minutes before commencing recordings. From these we were able to observe the propagation of cardiac waves across the plates by detecting the minute contractile motions of the myocytes. Frame rates were captured between at 50 fps. The software for displaying the camera output in real time, saving and analyzing data were written in a combination of Java and Python, and is directly available from the authors. For detailed description of the methods see (Burton *et al.*, 2015). To measure the effects of neuron stimulation on myocyte beat rate, 10 µM nicotine ([-] nicotine hydrogen tartrate salt; Sigma-Aldrich) was used to trigger depolarisations. Washout was performed with pre-warmed media (similar to the methods described by (Furshpan *et al.*, 1976)).

Imaging setup: We developed a dye free imaging system similar to that described in (Hwang et al., 2005), where off-axis oblique illumination is used to generate high contrast images that can be analysed to extract wave activity. We employ an Olympus MVX10 macroscope to relay a 1x image to a Neo sCMOS camera running at 50 frames/second. The high resolution of the camera allows visualization of the contraction of the tissue at the cell level, while still giving a relatively large 16 x 16 mm field of view. High resolution frames are processed so each displayed frame is generated by subtracting a frame captured at t-300 ms from the current frame and displaying the absolute value of each pixel. Intensity vs. time traces are obtained by 5x5 pixels in the image. The intensity vs. time traces typically have a double hump morphology which is due to contraction (first hump) followed by relaxation (second hump) of the tissue (Figure S 5 bottom right trace).

Wave speed measurement: We employed a semi-automated approach for finding cardiac waves in optical mapping recordings and measuring their speed of propagation. Data files are preprocessed by first extracting motion transients by finding the absolute value of the intensity differences for every pixel over a 6-frame rolling window (see Burton et al., 2015), and performing a 8x8 spatial binning operation to give a 256x256 pixel stack of frames. Wavefronts are visually identified by the operator, who draws a path perpendicular to the wavefront along the propagation direction. The software then calculates the 50% maximum intensity crossing time for two rectangular (10 x 20 pixel) ROIs positioned at the ends of the drawn path. A conduction velocity measurement is calculated based on the path length and ROI threshold crossing times. Several (an average 14) measurements are made at different locations and times for each record, and the 90th percentile of these is saved as a representative conduction velocity for that experiment. We compare conduction velocities from 22 co-culture and 19 myocyte only cultures. Normal distribution of the data was confirmed using the Kolmogorov-Smirnov test and data were compared using unpaired, twotailed t-test (P = 0.026, data shown as mean \pm SD). Our automated conduction velocity measurement system yields lower values than measurements of planar waves in paced tissue, which may be due to the inclusion of slowly moving highly curved wavefronts in the calculations (e.g. wave fronts near the core of a spiral wave). We note that the maximal

observed wave velocity in our preparations was 133 mm/second, which is similar to planar wave conduction velocities in isotropic tissue reported by other groups.

3] Simultaneous patch clamp electrophysiology-video recording: Current clamp was used to record electrophysiological traces from neurons, while video recording of cardiac behaviour was performed simultaneously using a CCD camera. The signal was recorded and analysed using custom-made procedures in Igor Pro (Wavemetrics). Image series were after processing the images so that the value of each pixel p at frame t, denoted p(t), is replaced by the absolute value of p(t) – p(t-5).

Current clamp recordings were performed with a Multiclamp 700B amplifier (Molecular Devices). Borosilicate glass pipettes were filled with an internal solution containing (in mM): 110 potassium-gluconate, 40 HEPES, 2 ATP-Mg, 0.3 GTP and 4 NaCl (pH 7.2–7.3; osmolarity 270–285 mOsmol). Standard artificial cerebrospinal fluid (ACSF) bubbled with 5% CO2 was used as the bath solution, containing (in mM): 126 NaCl, 3 KCl, 1.25 NaH2PO4, 2 MgSO4, 2 CaCl2, 26 NaHCO3, and 10 glucose, pH 7.2–7.4. All recordings were conducted at 37°C. Square pulses of current or current steps were administered to depolarise the neurons and elicit action potential firing. Data were low-pass filtered at 2 kHz and acquired at 5 kHz.

4] Assessment of cardiac activity in co-cultures with low neuron density using high throughput fluorescence methods on SBU culture: Caged-Nicotine:

Electrophysiological experiments studying the effects of noradrenaline release by sympathetic neurons on cardiac behaviour employ methods that flow on drug and monitor voltage or calcium changes either via the patch pipette or beat rate changes using video microscopy. We first tested the co-cultures using conventional pharmacological approaches (with Sigma 50 μM nicotine stimulation), to demonstrate the expected results of noradrenaline release by stellate sympathetic cardiac neurons on myocytes. Conventional methods such as the aforementioned do not offer any temporal or spatial control. Such a technique does not bode well with high-throughput imaging methods as the drug effect and the imaging timings cannot be precisely coordinated.

Due to technical challenges in co-culture patch clamp method, we performed a pilot study where a single patched neuron, driven to rapidly fire by injection of current, modulated the activity of a confluent monolayer. While this pilot experiment suggested that a single rapidly firing neuron can drive the behavior of a macroscopic cardiac monolayer, this protocol cannot rule out network effects from unpatched neurons. However, performing patch experiments on co-cultures with very few neurons (e.g. theoretically calculated one neuron per monolayer) was not practical as it proved to be technically difficult to locate a neuron amongst thousands of cardiomyocytes within an acceptable time frame. We therefore opted to investigate the activity co-cultures with low neuron numbers (calculated for 1 neuron:100,000 myocytes) using opto-chemical stimulation and a previously published high throughput fluorescent imaging technique (Klimas *et al.*, 2016). Since the low number of neurons increased variability, experiments were performed using multi-well plates to obtain sufficient statistical power. The use of multi-well plates necessitated the use of a modified experimental setup that differed from the one used to image activity in conventional petri plates as follows.

Due to temporal limitations of drug administration and effects, an alternative technique suitable to high-throughput measurements employing caged compounds was employed. Caged compounds are light-sensitive probes that functionally encapsulate molecules first introduced in the 1970's. These molecules are in an inactive form and upon irradiation, liberate the trapped molecule allowing targeted perturbation of physiological processes (Ellis-Davies, 2007). Caged nicotine known as RuBiNic (RuBi-Nicotine, Cat No. 3855, Tocris) has been used in neurotransmission studies (Filevich *et al.*, 2010a). Uncaging can be extremely rapid, controlled in time or space and quantitatively controlled and repeated. We tested the following neuron-myocyte densities: 1:5, 1:20 and 1:100,000 (see Figure S 4 for immuno-histochemistry staining of neurons at different neuron-myocyte co-culture ratios).

Opto-chemical neuronal stimulation and the effect of neurotransmitter release on cardiomyocytes:

Neonatal rat ventricular cardiomyocyte/co-cultures (SBU culture) were employed (see Supplementary Methods point 1b). Importantly, cardiac/co-cultures were maintained in low serum (2%) maintenance media from day 2. Optical recording of membrane voltage, Vm, was performed using the synthetic voltage-sensitive dye Di-4-ANBDQBS. 17.5 mM of stock solution in pure ethanol is diluted to 35 μ M Tyrode's solution. Cells are stained for 6 min in dye solution followed by a 6 min wash in fresh Tyrode's. Finally, the wash solution is replaced with fresh Tyrode's. SBU fluorescence imaging was performed at 200 fps with 4 × 4 binning using NIS-Elements AR (Nikon Instruments; Melville, NY). RuBi-Nicotine uncaging was elicited by a 150 ms, 1200 mA flash (470nm).

Neurons were stimulated using 100 μ M caged nicotine (Tocris, USA)(Filevich *et al.*, 2010a) instead of free nicotine in solution in order to minimize the time between sequential measurements in multiple wells. The concentration of free nicotine following photorelease in these experiments was less than the concentration of the caged nicotine used (100 μ M) as photorelease efficiency is poor at physiologically tolerated light levels. We tested the effects of caged nicotine between 10-100 μ M and found that 100 μ M resulted in neuronal driven cardiac responses similar to those evoked by the pure nicotine compound. We note that low photorelease efficiencies have been reported with similar compounds: Macgregor *et al.*, 2007 report a 2% efficiency of photorelease with caged NAADP (Macgregor *et al.*, 2007).

Neuronal optogenetics actuation:

The geometry of the multi-well plate (deep well relative to the bottom surface area) is not compatible with the oblique illumination method used for dye-free imaging used in larger plates due to unwanted light reflections of the sides of the well. In addition, the advantages associated with dye-free imaging (long term recording with low phototoxicity) are less relevant for these experiments as activity in different wells are measured in rapid succession for relatively short time periods. We therefore opted to measure cardiac activity using voltage-sensitive dye Di-4-ANBDQBS ($10~\mu M$, supplied by Dr Leslie Loew, University of Connecticut). A standard epi-fluorescence configuration was used (530~nm excitation light, with a 20x~objective (20~x~Nikon~CFO~Super~Plan~Fluor)).

The short time available for each recording and the microscopic field of view precludes measurement of CV and relatively subtle changes in patterns of activation. We therefore use experimental conditions that allow for an unambiguous assessment of the effects of nicotine on cardiac dynamics. For cell plating, 96-well glass bottom dishes (In Vitro Scientific) were coated with 50 μ g/mL fibronectin (diluted in PBS), and incubated at 37 °C for at least 2 h before cell plating. Cells are plated in 10% FBS M199 media; on day 2, the media was

replaced with 2% FBS M199 until the day of experiments and imaged at room temperature, which favors quiescent or slowly beating cultures (Klimas *et al.*, 2016). The co-culture in each well can then be labeled as responsive or un-responsive to nicotine based on the induction of activity in normally quiescent cultures or a marked increase in beat rate in slowly beating cultures. Wells that display rapid or irregular activity before the addition of nicotine are excluded from subsequent analysis.

Each well is plated with 140,000 cardiomyocytes and seeded with neurons at a concentration of 1 neuron per 100,000 myocytes (theoretical aim). At this plating density, Poisson statistics predict that 24.6% of plates will have zero neurons, 34.5% will have one neuron, and 40.9% will have more than one neuron. The number of wells that respond to nicotine is used to determine the number of neurons needed to induce activity in a connected monolayer.

Optogenetic modification of neurons: Adenoviral vectors containing the transgene for hChR2(H134R)-eYFP were prepared in collaboration with the Stony Brook University Stem Cell Centre based on the expression cassette of the plasmid pcDNA3.1/hChR2(H134R)-eYFP (#20940; Addgene) (Ambrosi and Entcheva, 2014). Neurons were infected using Ambrosi's method (Ambrosi and Entcheva, 2014) with an optimised dose of adenovirus (multiplicity of infection (MOI) 2000) at 37°C for 2 h. Neuron expressing ChR2 was confirmed by eYFP reporter visualization. Following infection, fresh culture medium was added with a medium change at 12 h and then every 48 h with functional measurements performed on the sample from day 5 onwards (similar to studies by (Shcherbakova et al., 2007, Larsen et al., 2016). Optical recording of membrane voltage, Vm, was performed using the synthetic voltagesensitive dye Di-4-ANBDQBS, spectrally compatible with ChR2. The light intensity threshold for ChR2 activation was obtained from previous studies (Ambrosi et al., 2015). For Optogenetic experiments: Optical stimulation (470 nm) was provided at pulse lengths of 1 to 5 sec, at 0.5 Hz, using irradiances of 0.5–1 mW/mm. Whilst a wide range of pulse durations were tried, most the data analysed are in the 1-5 sec long pulses, Figure 5 B(i) is 3 sec per pulse.

(i) Beat rate changes in response to neuronal ChR2 stimulation: Figure 5 A illustrates the co-culture methods and high throughput all-optical interrogation approach. High throughput fluorescent imaging protocols of "optoelectrical" (via ChR2, Bi) vs "optochemical" (via Caged Nicotine, C) neural stimulation. Rat cardiac sympathetic stellate neurons are optogenetically transformed to respond to light activation, this promotes action potential firing in myocytes (Fig 5 B(i)). ChR2 expression by eYFP reporter (green) at four different neuronal plating densities 1:5, 1:20, 1:100 and 1:100,000 were studied. Optogenetic stimulation via ChR2: (Figure S 15 C) in the myocyte only culture shows no beat rate response, whereas in the co-culture (Figure S 15 D), we observe a beat rate response during the periods of light stimulation. Figure S 15 E, post processed traces using using custom-written Matlab software, where blue is the median filtering trace, red indicates detected spike times, black is an indicator of when light is present (black up=light on, 3 sec pulse).

Optochemical stimulation of neurons with nicotine (Figure S 16 B (ii): pre-uncaging, B (iii): post-uncaging, B (iv): returning to baseline after several minutes of uncaging) and optoelectrical stimulation of neurons via ChR2 (Figure S 15 E), demonstrate functional coupling between neurons and myocytes in co-cultures. We additionally test this coupling by traditional pharmacological antagonists (nicotine, Figure S 17). Genetically modified sympathetic neurons with ChR2 co-cultured with myocytes can be optically stimulated to

drive a monolayer of myocytes (Figure S 15 F (i)) and this effect can be blocked using a beta-blocker (metoprolol, Sigma Aldrich, Figure S 15 F (ii)).

(ii) Cardiomyocyte response to ChR2 stimulation with ChR2-expressing neurons as a function of neuron density: Stimulating the ChR2-CSSN (cardiac sympathetic stellate neurons) elicits a rate response in the cardiac monolayer. The number of neurons innervating the myocytes affects the firing frequency of myocytes. Different neuronal plating densities influence the cardiac response. We observe a dose-dependent effect (i.e. the greater the number of neurons innervating the myocytes, the greater the effect; Figure 5 B (ii)).

Firing frequency versus concentration of neurons in co-cultures: There is a fairly strong dose-dependent effect observed, (Figure 5 B (ii)). We observe that most values are >0, indicating a speed up. Where x axis represents ratios of neurons to myocytes (0= myocytes/controls, 1e-05=1:100,000, 0.01=1:100, 0.05=1:20 and 0.2=1:5). No significant increase/decrease observed with light stimulation in controls (no neurons) versus co-cultures. All data analysed using custom-written Matlab script.

(iii) Validation of a co-culture model and translational value- iPSc-CM and iPSc-peripheral neurons:

The data we present are more anecdotal due to the limited n numbers. Example traces, and response to caged nicotine and optogenetic manipulation of iPSc-derived peripheral neurons with immunostains are presented to demonstrate the utility of the methodology presented in this paper. Cardiomyocyte response to ChR2 stimulation with ChR2-expressing peripheral neurons (MOI 2000) as a function of neuron density and blue light protocol of 3 sec on/off protocols were employed. Our data demonstrate the utility and power of our co-culture model and the applicability of high throughput fluorescent techniques (Klimas *et al.*, 2016) for contactless optogenetics experiments required in cell specific perturbations (Figure S 18). Cor.4U® human iPS-derived cardiomyocytes and Peri.4U® human iPS-derived peripheral neurons were grown as described by Axiogenesis handling guides (https://ncardia.com/resources/#manuals).

Here we performed direct adenoviral gene delivery in human iPSc-derived peripheral neurons (ChR2-hiPSc-PN, obtained from Axiogenesis) and observe the cardiac response to light stimulation of neurons (Figure S 18 D), confirming that optogenetic stimulation of cocultures is a suitable method and alternative for dissecting neural mediated cardiac function in a 'petri-dish'. To confirm the myocyte-like properties of the iPS-dervied cardiomyocytes, we utilised mouse anti-α-actinin primary antibody and imaged them using a confocal microscope, using the Olympus FluoView FV1000 system. All samples were fixed in 3.7% formaldehyde after performing functional experiments. Cells were permeabilised using 0.02% TritonX-100 for 5 minutes. Antibodies were diluted using 1% bovine serum albumin (Amersham PLC, Amersham, UK). 1% FBS was used as a blocking agent. After antibody staining, cell nuclei were stained with 1 µg/mL DAPI with 10 min incubation in PBS. From gene chip data provided by Ncardia, the iPSc-peripheral neurons Peri.4U have a high expression of Th gene (7719 where 501-1000 = high expression levels); and very low expression levels of ChAT gene (123, where <150 = absent/very low expression). The commercial cardiomyocytes used in the study (Cor.4U [Axiogenesis AG] was believed to be derived from human induced pluripotent stem cells during these studies. After studies had been completed short tandem repeat (STR) testing determined that the cell product was derived from the human embryonic stem cell line RUES2. Regarding Peri.4U; there is no evidence of the use of human embryonic stem cell lines.

- **5] Measurement of conduction velocity in well-connected SBU cultures with optical mapping:** Cardiac myocytes were cultured using the methods described in (Ambrosi *et al.*, 2015) and grown in glass bottom 35mm poly-lysine-coated Petri dishes (bio coat poly-Dlysine, 35 mm Petri plates, Corning; n=6). Neurons were isolated using the same methods described above. Co-cultures were created using different myocyte-neuron concentrations (20:1 n = 6, 100:1 n = 4, 600K:1 n=6). Using conventional optical mapping methods, we measured conduction velocity in well-connected cardiac cultures and co-cultures utilizing the dye Rhod-4-AM (10 μM: AAT Bioquest, Sunnyvale, CA). Rhod-4 AM diluted in Tyrode's solution containing the following in mM: NaCl, 135; MgCl₂ 1; KCl, 5.4; CaCl₂, 1.5; NaH₂PO₄, 0.33; glucose, 5; and HEPES 5 adjusted to pH 7.4 with NaOH. All experiments were conducted at room temperature. Details for the macroscopic imaging system used in this experiment has been described previously (Jia *et al.*, 2011). Data was spatially and temporally filtered, using the Bartlett and Savistsky-Golay filters, before being analyzed in custom-developed Matlab (Mathworks, Natick, MA) software.
- 6] Structural studies (confocal microscopy and scanning electron microscopy): Scanning electron microscopy (SEM): Co-cultures were prepared for SEM using a protocol adapted from (Bozzola, 2007). Briefly, cells were grown on 13 mm glass coverslips and fixed in 2.5% glutaraldehyde, post-fixed in 1% osmium tetroxide at 4°C for 1 hr, taken through an ethanol dehydration series and then dried for 3 minutes with HMDS. Cover-slips were mounted onto SEM stubs with a conductive carbon backing, coated with approximately 8 nm gold and imaged on a JEOL-6390 SEM (Figure 1).

Confocal microscopy: Briefly, cells were grown on 12 mm Poly-D-Lysine/Laminin coated coverslips (BD biosciences, UK) and fixed in 4% paraformaldehyde (Pierce Cat#28906) Following fixation, the cultures were washed in PBS and blocked with 10% goat serum and 0.3% BSA, and permeabilised with 0.1% Triton X-100 for 1 hour at room temperature. Cells were labelled with anti-sacromeric alpha actinin (1:650 A7811, SigmaAldrich, UK), anti-tyrosine hydroxylase (1:250 T1299, Sigma Aldrich), anti-beta2 adrenergic receptor (1:100, ab182136, Abcam, UK) and anti-Vimentin (1:250 ab92547, Abcam, UK) primary antibodies overnight at 4°C to confirm the presence of sympathetic neurons in co-cultures and to assess the growth of fibroblast in culture with Vimentin. Secondary fluorescent antibodies (Alexa 488 and 647, 1:1000) were then applied for 2 h at room temperature (controls were labelled with secondary antibody only to ensure specificity of labelling, Supplementary Figure S 2 and S 3). Slides were mounted in Vectashield to reduce photobleaching of fluorescence. Cultures were imaged using confocal microscopy (NT confocal laser-scanning microscope, Leica Microsystems Germany).

Measurement of neurite length and calculation of distance between cell boundaries:

	neurite	number
SEM	length	of cell
image #	(μm)	bodies
1	1523.22	1
3	9197.809	5
11	4893.733	5
17	8144.326	8
21	7000.653	7
total	30759.74	26
	average	
	length	
	(μm)	std
	1183.07	375.42

Measuring neurite length: SEM images were calibrated in ImageJ (Schneider et al., 2012) using their scale bars. Using the segmented line tool, neurite lengths were segmented, tabulated, and measured (Supplementary Figure S 1). Cell bodies were classified by: (i) cell body morphology (ii) size and (iii) arborisations confirmed by a Specialist in Anatomy, Prof Helen Christian (Oxford). The average neurite length is computed as a weighted average, $1183.07 \pm 375.42 \,\mu m$, from the data shown in the table above.

Calculating distance between cardiomyocyte cell boundaries: A confocal image stack of fluorescently labelled cardiomyocytes (TH488) was used as the starting point for the image analysis (Fig 2 A (i)). A maximum intensity projection was taken of the image stack before manually segmenting the CM cell boundaries (Fig 2 A(ii)). The image was thresholded and binarised to leave only the cell boundaries on a black background. A computer script then identified random start and end points for transects across this segmented image with a fixed length of 50 microns. All transects starting or terminating outside of the image boundaries were rejected. The intensity profile along each random transect was then used to identify the number of times a cell boundary was crossed ('N'). By dividing 50 μm by N it is possible to estimate the typical distance between cell boundaries for a random transect across the cardiac monolayer.

7] Proteomics:

(i) In-gel trypsin digestion

Cell lysates were mixed with an equal volume of reducing SDS-PAGE sample buffer, heat denatured (95°C for 10 min) and run into the upper part of a Tris-Glycine 8-16% gel (185V, 10m min). Protein material was excised after Coomassie blue staining and cut into $1-2~{\rm mm}^3$ gel pieces, which were placed into 1.5 mL sample tubes. Gel pieces were rinsed twice with wash solution for 18h in total (200 μ l, 50% methanol, 5% acetic acid). The solutions were removed and gel pieces were dehydrated in acetonitrile (200 μ l, 5 min). Supernatant were removed and gel pieces were dried in a vacuum centrifuge for 3 min. Disulfide reduction was performed with 10 mM DTT (30 μ l) for 0.5 h, followed by alkylation with 100 mM iodoacetamide (30 μ l) for 0.5 h. Supernatants were removed from the gel samples and dehydration with acetonitrile and evaporation performed as described above. Gel pieces were washed with 100 mM ammonium bicarbonate (200 μ l, 10 min). Supernatants were removed and dehydration performed with acetonitrile and evaporation as above. The gel samples were then rehydrated on ice with freshly prepared trypsin solution (30 μ l, 20 ng/ μ l sequencing grade trypsin [Promega] in 50 mM ammonium bicarbonate). After rehydration excess trypsin

solution was removed and 50 mM ammonium bicarbonate (10 μ l) was added to prevent dehydration of gel pieces. Gel samples were digested at 37°C for 18h. The gel pieces were then extracted sequentially with 50mM ammonium bicarbonate (60 μ l), 50% acetonitrile, 5% formic acid (60 μ l) and 85% acetonitrile, 5% formic acid (60 μ l). The combined extracts were evaporated in a vacuum centrifuge and were redissolved in 5% acetonitrile, 0.1% formic acid (20 μ l) on an ultrasonic bath and transferred into LC-MS sample vials.

(ii) Proteomics analysis by liquid chromatography-tandem mass spectrometry (LC-MS/MS) Trypsin digested samples were analyzed either on an Amazon Ion Trap mass spectrometer (Bruker Daltonics) as described previously (Kar *et al.*, 2014), or on Q-Exactive (Thermo Scientific) Hybrid Quadrupole-Orbitrap mass spectrometer LC-MS/MS system as detailed below.

Liquid chromatography: A Dionex UltiMate3000 RSLCnano pump at 300 nL/min flow rate was used for analytical separation of digested peptides. A C18, 75 μ m x 50 cm (2.6 μ m particle size, 150 A; part number: 16126-507569 Thermo Scientific) analytical column was used for separation of peptides and the column temperature was 50°C. Mobile phase used was: A – 0.1% v/v formic acid in water (LC-MS grade) and B – 0.1% v/v formic acid in acetonitrile (LC-MS grade). Two hours linear gradient was used as below, a multistep gradients between 121-132 minutes were used to remove any carryover.

Time	$^{\rm MB}$	Flow (nL/min)
0-3.1	3	300
3.1-120	40	300
121-125	90	300
126-128	3	300
129-132	90	300
133-158	3	300

A Dionex UltiMate 300 RS pump was used for desalting the peptide. A C18 PepMap (μ-Precolumn, 300 μM I.D. x 5 mm, 100 μm particle size, 100 A; Part number: 160454, Thermo Scientific) trapping column was used for trapping peptides. Buffer used for trapping and desalting peptides was 0.05% v/v Trifluoroacetic acid (TFA) in water (LC-MS grade). 1 μl of samples was injected and allowed for desalting for 3 minutes at 10 μl/min flow rate. After 3 minutes of desalting the trapping valve was changed and directed (backward flush) to analytical column for separation of all trapped peptides on trapping column.

(iii) Mass spectrometry: A bench top Q-Exactive (Thermo Scientific) Hybrid Quadrupole-Orbitrap mass spectrometer was used for data acquisition. A Top10 data dependent acquisition (DDA) method was used. Mass spectrometer was calibrated, for mass accuracy using positive ion calibration mixture provided by mass spectrometer manufacturer, prior to data acquisition. The conditions for the DDA mode were; Chromatographic peak width: 10 s, the Full MS conditions used- resolution: 70,000, AGC target: 1e6, maximum IT (injection time): 100 ms, scan range: 300 to 2000 m/z. The dd-MS2 conditions - resolution: 17,500. The AGC target conditions- 5e4, maximum IT: 100 ms, loop count: 10 (i.e. Top 10), isolation width: 1.6 m/z, fixed first mass: 120.0 m/z, and the data dependent (dd) settings -under fill ratio: 10% (it sets up a minimum intensity threshold of 5e4 ions), charge exclusion: unassigned, 1, 8, >8, peptide match; preferred, dynamic exclusion: 30 s. Normalised Collison Energy (NCE) of 27 was used for fragmentation of peptides in a high-energy collision dissociation (HCD) cell. This method allows the selection, fragmentation and detection of ten precursors in a duty cycle time of 1.42 s.

(iv) Data processing and database searching: For the analyses carried out using the Amazon Ion Trap (Bruker Daltonics), raw LC-MS/MS data were processed and Mascot compatible files were created using DataAnalysis 4.0 software (Bruker Daltonics). Database searches were performed using the Mascot algorithm (version 2.5.1) and the UniProt_SwissProt database with taxonomy restriction 'rat' (v2015.02.04, number of entries 547,357, after taxonomy filter: 7,930). The following parameters were applied: 2+, 3+ and 4+ ions, peptide mass tolerance 0.3 Da, 13C = 2, fragment mass tolerance 0.6 Da, number of missed cleavages: two, instrument type: ESI-TRAP, fixed modifications: Carbamidomethylation (Cys), variable modifications: Oxidation (Met).

For the analyses carried out using the Q-Exactive (Thermo Scientific) Hybrid Quadrupole-Orbitrap mass spectrometer, LC-MS/MS data (.raw files) were converted to .mgf files and Database searches were performed using the Mascot algorithm (version 2.5.1) and the UniProt_SwissProt database with taxonomy restriction 'rat' (v2015.11.26, number of entries after taxonomy filter: 7,954). The following parameters were applied: 2+, 3+ and 4+ ions, peptide mass tolerance 10 ppm, 13C = 2, fragment mass tolerance 0.06 Da, number of missed cleavages: two, instrument type: Q-Exactive, fixed modifications: Carbamidomethylation (Cys), variable modifications: Oxidation (Met).

Protein quantification was performed by spectral counting using the SINQ method (Trudgian *et al.*, 2011). Protein ratios (co-cultures/myocytes) were calculated from SINQ intensities for all quantified protein hits. We chose a 3 -fold change as a threshold for regulation (Protein SINQ Quantitation data provided in Supplementary Tables 5 and 6).

(v) Gene ontology enrichment analysis of the clusters in the network: This was performed for the protein networks obtained by linking the mass spectrometry results (Table 1 and 2) with STRING database.

The following tool was used for the analysis:

https://www.psb.ugent.be/cbd/papers/BiNGO/Home.html

Gene ontology used was from: http://geneontology.org/docs/download-ontology/ The gene ontology has 3 sub-ontologies:

- 1. Biological Process (BP)
- 2. Cellular Component (CC)
- 3. Molecular Function (MF)

We ran over-representation tests for all proteins for all three categories (Supplementary Table 3 and 4).

Supplementary Table 3 has the following structure:

-tab ST3A) 22SDallclusters-BP - this contains the Bingo hypergeometric tests against the Biological Process (BP) gene ontology for 22SD experiment

-tab ST3B) 22SDallcluster-CC - this contains the Bingo hypergeometric tests against the cellular component (CC) gene ontology for 22SD experiment

-tab ST3C) 22SDallcluster-MF - this contains the Bingo hypergeometric tests against the molecular function (CC) gene ontology for 22SD experiment

Supplementary Table 4 has the following structure:

-tab ST4A) SDCN5allclusters-BP - this contains the Bingo hypergeometric tests against the Biological Process (BP) gene ontology for SDCN5 experiment

-tab ST4B) SDCN5allclusters-CC - this contains the Bingo hypergeometric tests against the cellular component (CC) gene ontology for SDCN5 experiment -tab ST4C) SDCN5allclusters-MF - this contains the Bingo hypergeometric tests against the molecular function (MF) gene ontology for SDCN5 experiment

Insights from Proteomics: Proteomics highlights changes in cytoskeletal, metabolic and nuclear proteins which occur in co-cultures: To further shed light on the molecular mechanisms governing the difference in macroscopic behaviour, we looked at the protein expression profiles between the two cultures. We performed a comparative proteome analysis of harvested cell cultures. Database searches of merged peak list files were carried out using the MASCOT algorithm with taxonomy restriction to rat sequences. False-discovery rate (FDR) estimation was performed through a target-decoy search strategy and all results were displayed at a FDR of $\leq 1\%$ (Supplementary Table 1).

The identified proteins included many abundant cytoskeletal proteins (actin, tubulin, vimentin, vinculin, actinin), metabolic enzymes (alpha-enolase, GAPDH, pyruvate kinase, ATP synthase) and nuclear proteins (histones H2A, H2B, H3, H4, prelamin) which were detected commonly across the two samples.

Among the most strongly regulated protein hits we see a significant increase in several biological processes (See Figure S 8 and S 10) from 2 independent experiments). From the STRING (Jensen *et al.*, 2009) and Expressence analysis, the most abundant class of proteins in the co-cultures can be seen in Supplementary Table 3 and 4, Enrichment Analysis for two independent samples (SD5 and SD22, significance <0.05). Interestingly, using the Cellular Component analysis (Supplementary Table 3 and 4, tab abbreviated CC), we observe a significant up regulation in translational and mitochondrial related proteins including mitochondrial respiratory chain complex III (Supplementary Table 3 and 4, tab CC, and visualised in Figure S 8 and S 10).

Western blot studies: Western blots of Connexin43 expression in 2 separate culture experiments grown in the absence and presence of sympathetic cardiac stellate neurons (Sprague Dawley (SD) and Wistar Kyoto (WKY) animals), Supplementary Figure S 12. Cell lysate was heated to 95°C for 5 min (to denature the protein) and vortexed before 20 µg was loaded into a 4-12% Tris-Glycine gel. The gel was run for 150 minutes at 125 V. After electrophoretic transfer (2 hours, 40 V) to a membrane (nitrocellulose), the membrane was washed with Tris Buffered Saline (TBS: 50 mM Tris-CI, 150 mM NaCl, pH 7.6) and blocked for an hour using a 5% milk solution (in TBST: TBS with 0.1 % Tween20). The primary antibody (Connexin 43, AB1728, Millipore, UK; 1:200) in 5% milk solution was incubated for 60 min at room temperature on a rocker. The membrane was washed three times in TBST at intervals of 10 minutes and incubated with a horse radish peroxidase (HRP)-conjugated secondary antibody (anti-mouse IgG 1:10000, anti-rabbit IgG 1:10000; both Novus Biologicals) in TBST solution for 60 minutes, then subjected to three washes at 10 minute intervals using TBST. Next, the membrane was washed twice for 10 minutes in distilled water for to ensure complete removal of tween which could interfere with HRP reaction. The ECL+ kit (Perkin Elmer Western Lightning ECL Pro, NEL120001EA) was used and a series of exposures using photographic film was collected. This was repeated with a GAPDH antibody, the loading control, (1:2500, Abcam, ab181602). Optical densitometry of the western blots was conducted using ImageJ software. Connexin43 (Cx43) levels in cultures using Western blot technique (Figure S 12) confirmed that Cx43 was higher in the co-cultures (two independent experiments).

8] Statistics: Details provided in each result and online methods. Data are presented as means \pm -stdev. In all cases P < 0.05 was considered to indicate a statistically significant difference. The chi-square statistic was used to assess differences in pattern formation. The Kolmogorov-Smirnov test was used to assess normal distribution and subsequent comparison was run using unpaired, two-tailed t-test (P = 0.026) for the automated measurement of wavefront speed. The t-test was used to assess patch clamp results. ANOVA followed by Tukey-Kramer was used for well-connected mono and co-culture conduction velocity statistical tests.

References

- Ambrosi, C. M., Boyle, P. M., Chen, K., Trayanova, N. A. & Entcheva, E. 2015. Optogenetics-enabled assessment of viral gene and cell therapy for restoration of cardiac excitability. *Sci Rep.* 5, 17350.
- Ambrosi, C. M. & Entcheva, E. 2014. Optogenetic control of cardiomyocytes via viral delivery. *Methods Mol Biol*, 1181, 215-28.
- Bozzola, J. J. 2007. Conventional specimen preparation techniques for scanning electron microscopy of biological specimens. *Methods Mol Biol*, 369, 449-66.
- Burton, R. A., Klimas, A., Ambrosi, C. M., Tomek, J., Corbett, A., Entcheva, E. & Bub, G. 2015. Optical control of excitation waves in cardiac tissue. *Nat Photonics*, 9, 813-816.
- Ellis-Davies, G. C. 2007. Caged compounds: photorelease technology for control of cellular chemistry and physiology. *Nat Methods*, 4, 619-28.
- Filevich, O., Salierno, M. & Etchenique, R. 2010a. A caged nicotine with nanosecond range kinetics and visible light sensitivity. *J Inorg Biochem*, 104, 1248-51.
- Filevich, O., Salierno, M. & Etchenique, R. 2010b. A caged nicotine with nanosecond range kinetics and visible light sensitivity. *Journal of Inorganic Biochemistry*, 104, 1248-1251.
- Furshpan, E. J., MacLeish, P. R., O'Lague, P. H. & Potter, D. D. 1976. Chemical transmission between rat sympathetic neurons and cardiac myocytes developing in microcultures: evidence for cholinergic, adrenergic, and dual-function neurons. *Proc Natl Acad Sci USA*, 73, 4225-9.
- He, Y. & Baas, P. W. 2003. Growing and working with peripheral neurons. *Methods Cell Biol*, 71, 17-35.
- Hwang, S.-m., Kim, T. Y. & Lee, K. J. 2005. Complex-periodic spiral waves in confluent cardiac cell cultures induced by localized inhomogeneities. *Proceedings of the National Academy of Sciences of the United States of America*, 102, 10363-10368.
- Jensen, L. J., Kuhn, M., Stark, M., Chaffron, S., Creevey, C., Muller, J., Doerks, T., Julien, P., Roth, A., Simonovic, M., Bork, P. & von Mering, C. 2009. STRING 8--a global view on proteins and their functional interactions in 630 organisms. *Nucleic Acids Res*, 37, D412-6. Jia, Z., Valiunas, V., Lu, Z., Bien, H., Liu, H., Wang, H. Z., Rosati, B., Brink, P. R., Cohen, I. S. & Entcheva, E. 2011. Stimulating cardiac muscle by light: cardiac optogenetics by cell
- Kar, P., Samanta, K., Kramer, H., Morris, O., Bakowski, D. & Parekh, A. B. 2014. Dynamic assembly of a membrane signaling complex enables selective activation of NFAT by Orai1. *Current biology: CB*, 24, 1361-1368.
- Klimas, A., Ambrosi, C. M., Yu, J., Williams, J. C., Bien, H. & Entcheva, E. 2016. OptoDyCE as an automated system for high-throughput all-optical dynamic cardiac electrophysiology. *Nat Commun*, 7, 11542.

delivery. Circ Arrhythm Electrophysiol, 4, 753-60.

- Larsen, H. E., Lefkimmiatis, K. & Paterson, D. J. 2016. Sympathetic neurons are a powerful driver of myocyte function in cardiovascular disease. *Sci Rep*, 6, 38898.
- Li, D., Lee, C. W., Buckler, K., Parekh, A., Herring, N. & Paterson, D. J. 2012. Abnormal intracellular calcium homeostasis in sympathetic neurons from young prehypertensive rats. *Hypertension*, 59, 642-9.
- Macgregor, A., Yamasaki, M., Rakovic, S., Sanders, L., Parkesh, R., Churchill, G. C., Galione, A. & Terrar, D. A. 2007. NAADP controls cross-talk between distinct Ca2+ stores in the heart. *J Biol Chem*, 282, 15302-11.
- Shcherbakova, O. G., Hurt, C. M., Xiang, Y., Dell'Acqua, M. L., Zhang, Q., Tsien, R. W. & Kobilka, B. K. 2007. Organization of β-adrenoceptor signaling compartments by sympathetic innervation of cardiac myocytes. *The Journal of Cell Biology*, 176, 521-533.

Trudgian, D. C., Ridlova, G., Fischer, R., Mackeen, M. M., Ternette, N., Acuto, O., Kessler, B. M. & Thomas, B. 2011. Comparative evaluation of label-free SINQ normalized spectral index quantitation in the central proteomics facilities pipeline. *Proteomics*, 11, 2790-2797.

SUPPLEMENTARY FIGURES

Figure S 1: Measuring neurite length in wide field Scanning electron microscopy (SEM) images of co-cultures, related to Figure 1. SEM images were calibrated in ImageJ using their scale bars. Using the segmented line tool, neurite lengths were segmented, tabulated, and measured. Cell bodies were classified by morphology and dendritic arborisation.

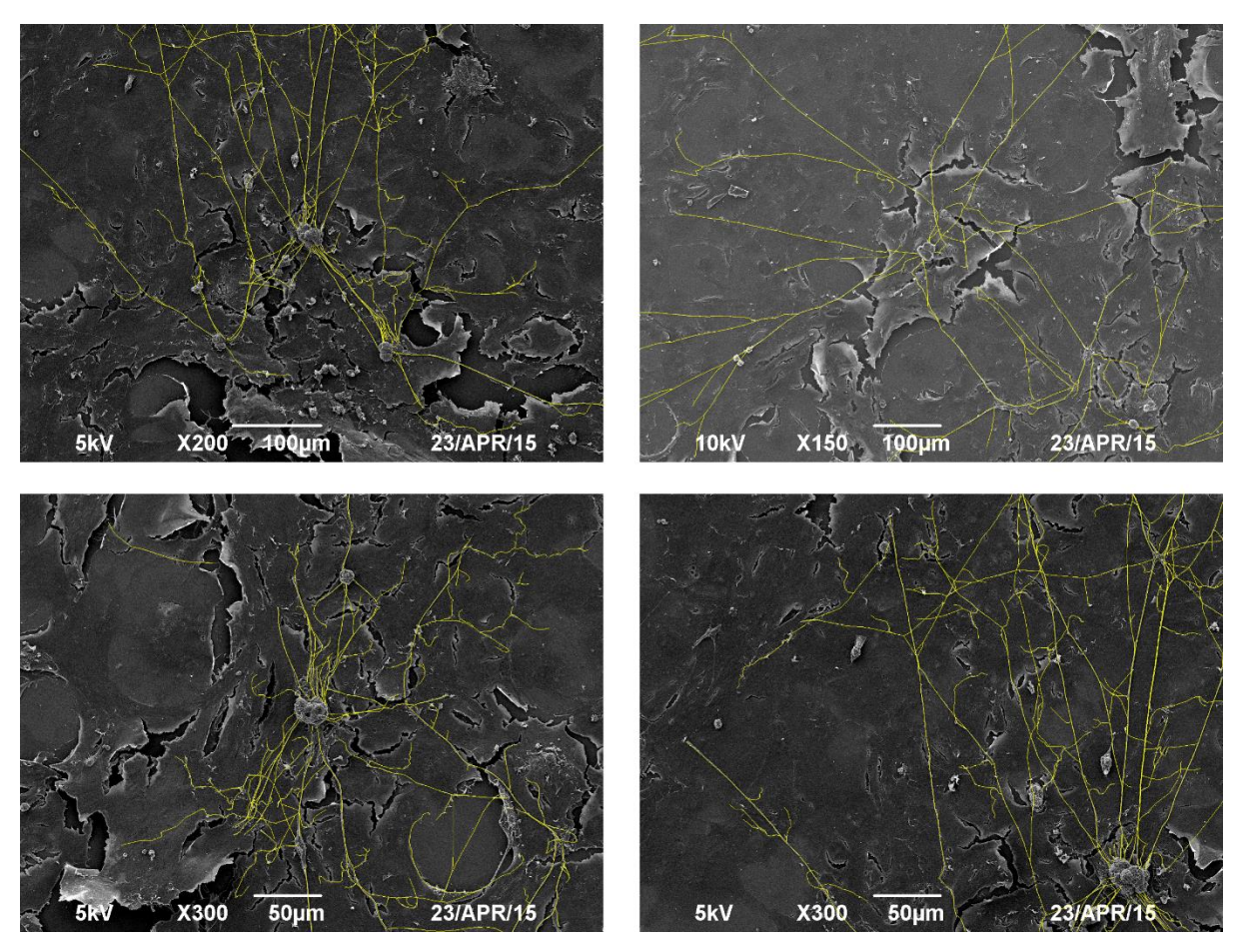


Figure S 2: Co-cultures of ventricular myocytes and sympathetic stellate neurons, related to Figure 1 and 2. Immunofluoresence staining confirmed sympathetic neurons with Tyrosine hydroxylase (TH - red), which is a sympathetic neuron marker. The neuronal processes interweave with the myocytes resulting in a rich innervation of the cardiac myocytes. Th and DAPI (blue) co-staining on co-cultures. Scale bars 20 μ m.

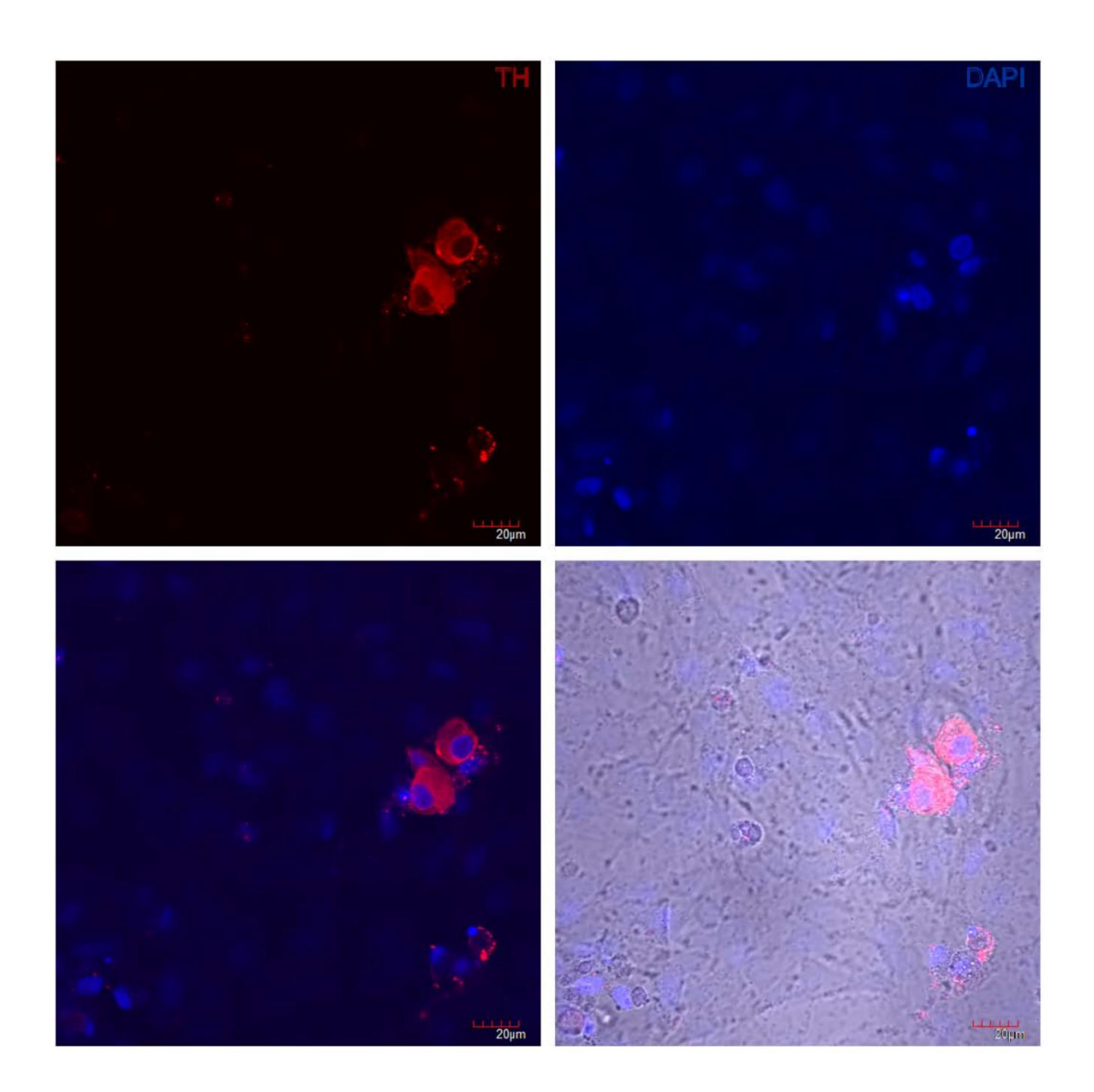


Figure S 3: Co-cultures of ventricular myocytes and sympathetic stellate neurons, related to Figure 1 and 2. Immunofluoresence staining to assess the amount of fibroblasts with Vimentin marker (red), alpha actinin marks the myocytes (green). DAPI (blue) stain on co-culture to identify cell nuclei. Scale bars 20 μ m.

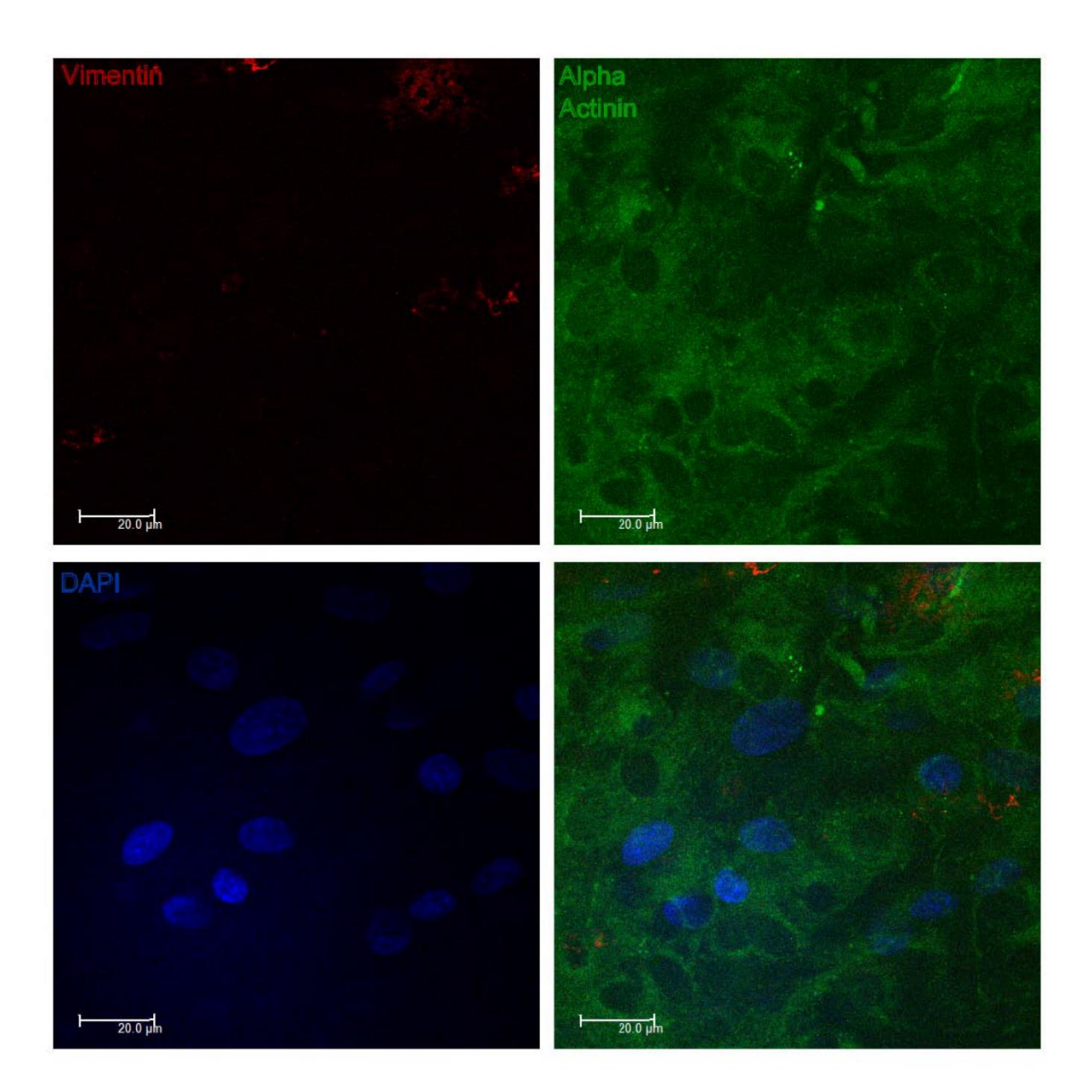


Figure S 4: Co-cultures of ventricular myocytes and sympathetic stellate neurons, related to Figure 1, 2 and 5. Cardiac sympathetic stellate neurons were plated on top of monolayer of ventricular myocytes. Immunofluoresence staining confirmed the sympathetic neurons. Tyrosine hydroxylase (TH – red) is a sympathetic neuron marker. The neuronal processes naturally interweave with the myocytes as seen in the brightfield images resulting in a rich innervation of the myocytes. Immunohistochemistry analyses using TH (red) antibody in the different neuron-myocyte co-culture ratio combinations ((i) 1:5, (ii) 1:20, (iii) 1:100 and (iv) 1:100,000).

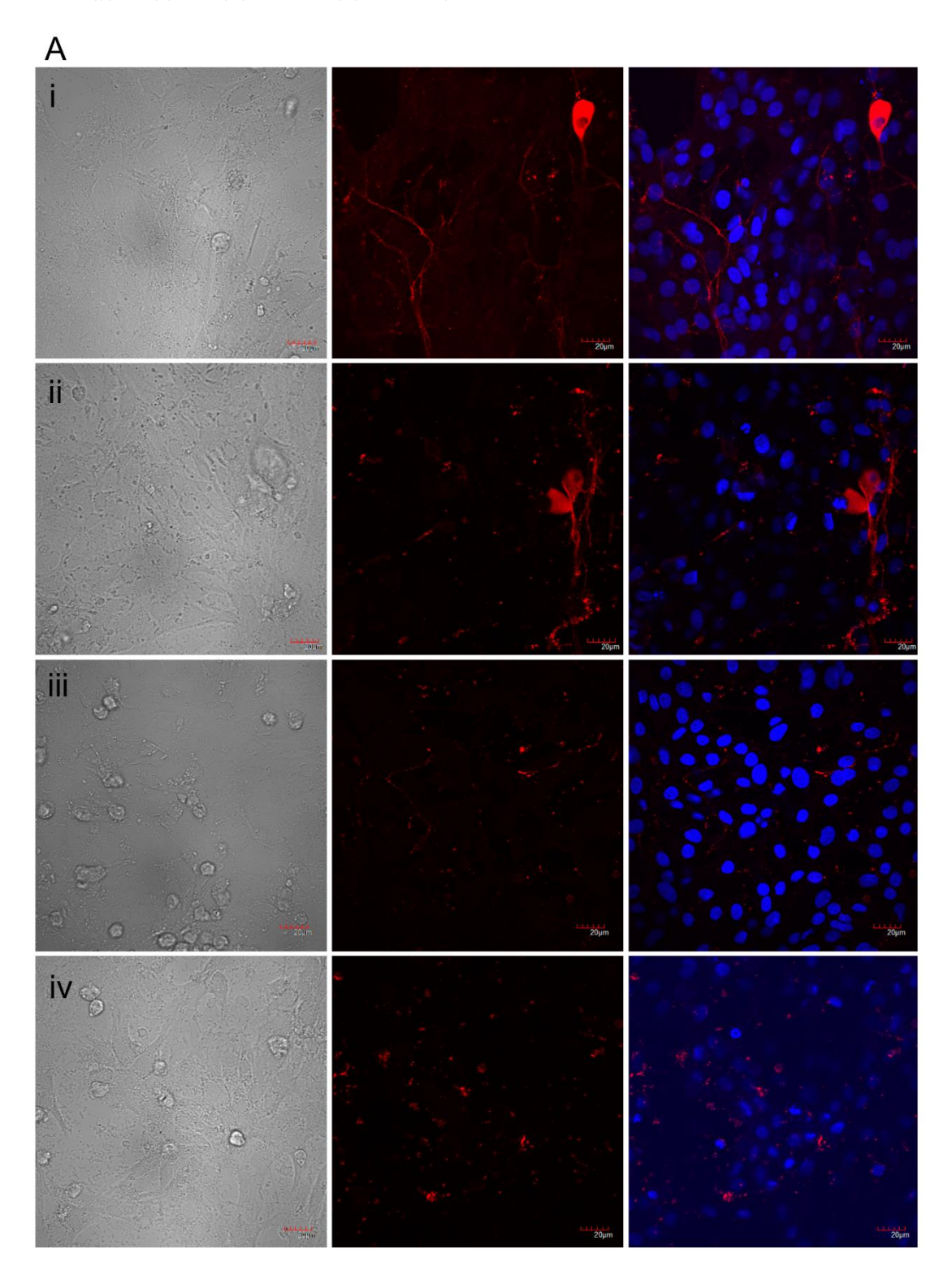


Figure S 5: Off-axis illumination imaging to obtain high contrast images of the monolayer, related to Figure 2 B. Images are processed to calculate the absolute value of the intensity change over n frames. Unfiltered image (Top panel), Note: The image is obtained using a 10x lens instead of the 1x used for the main dye free experiments. (middle and bottom left and right panels) Filter applied to track motion in the cardiac monolayer, traces below, intensity vs time plots for the central 5x5 pixels in the image [Filter: Pt(x,y)Pt-N(x,y)]. The left trace shows intensity from unprocessed images and the right trace show the improved s/n after processing.

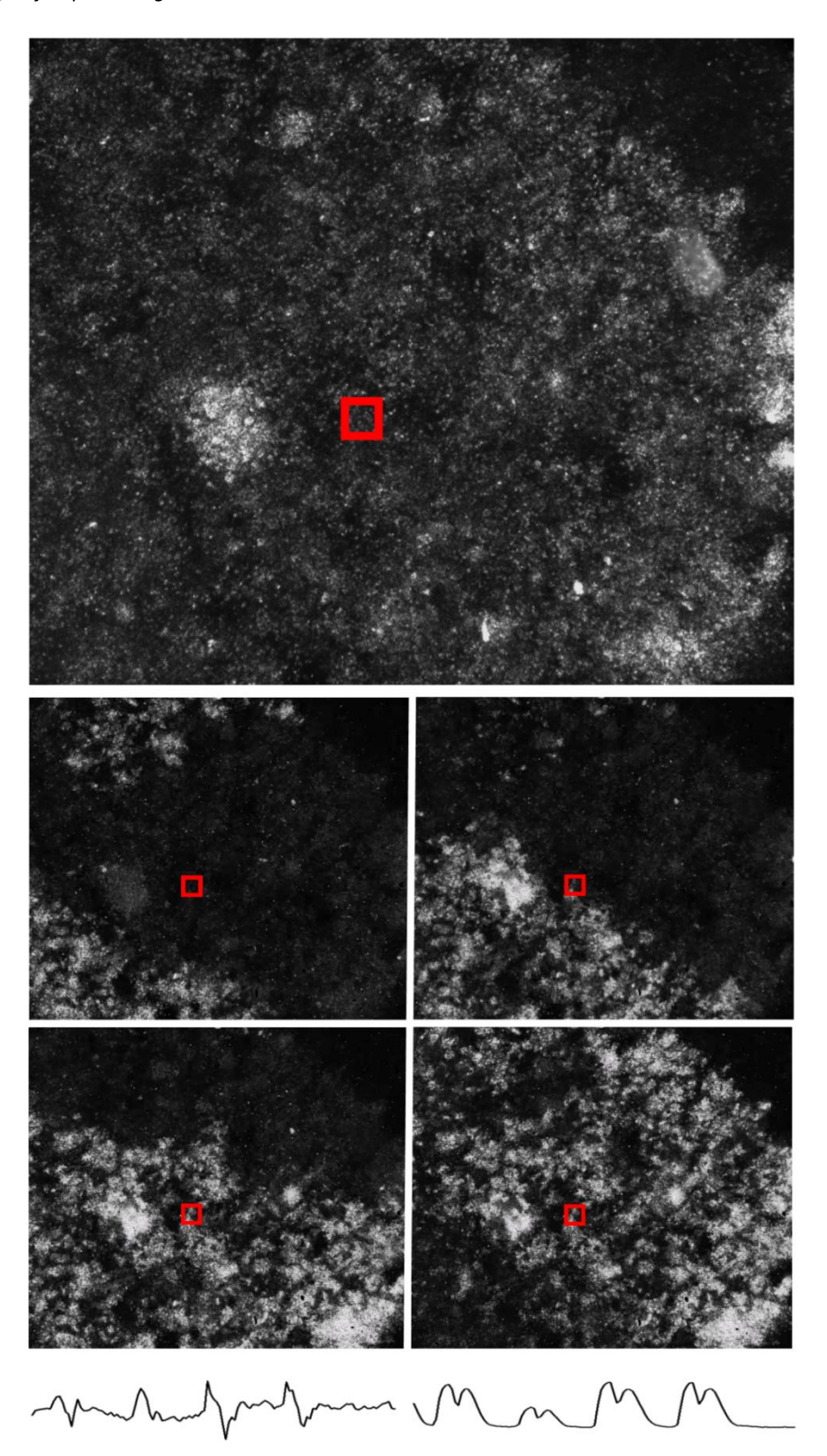


Figure S 6: Individual frames from a video recorded before and after nicotine application, related to Figure 4. The video was processed to show motion transients (white) as described in the supplement. Changes in cardiac macroscopic activity correlate with neuronal bursting following nicotine application. Camera frame rate: 17.5Hz. Each frame pictured represents $119 \, \mu m^2$.

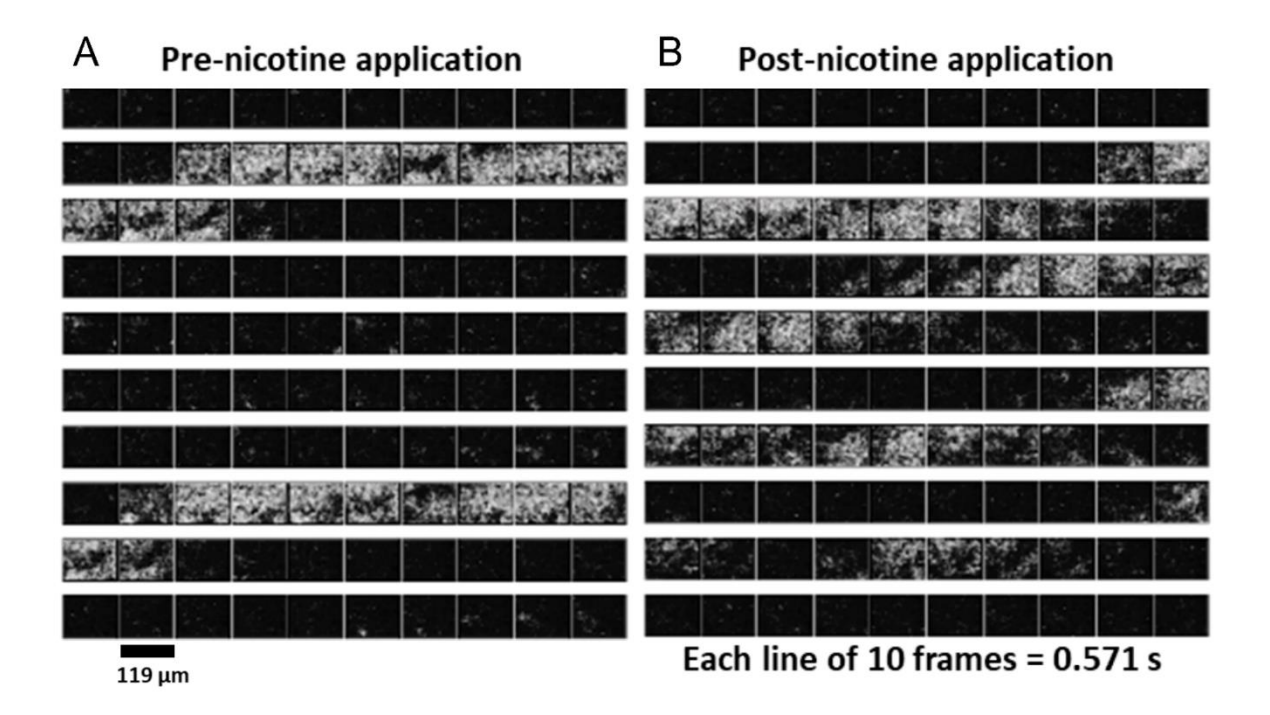
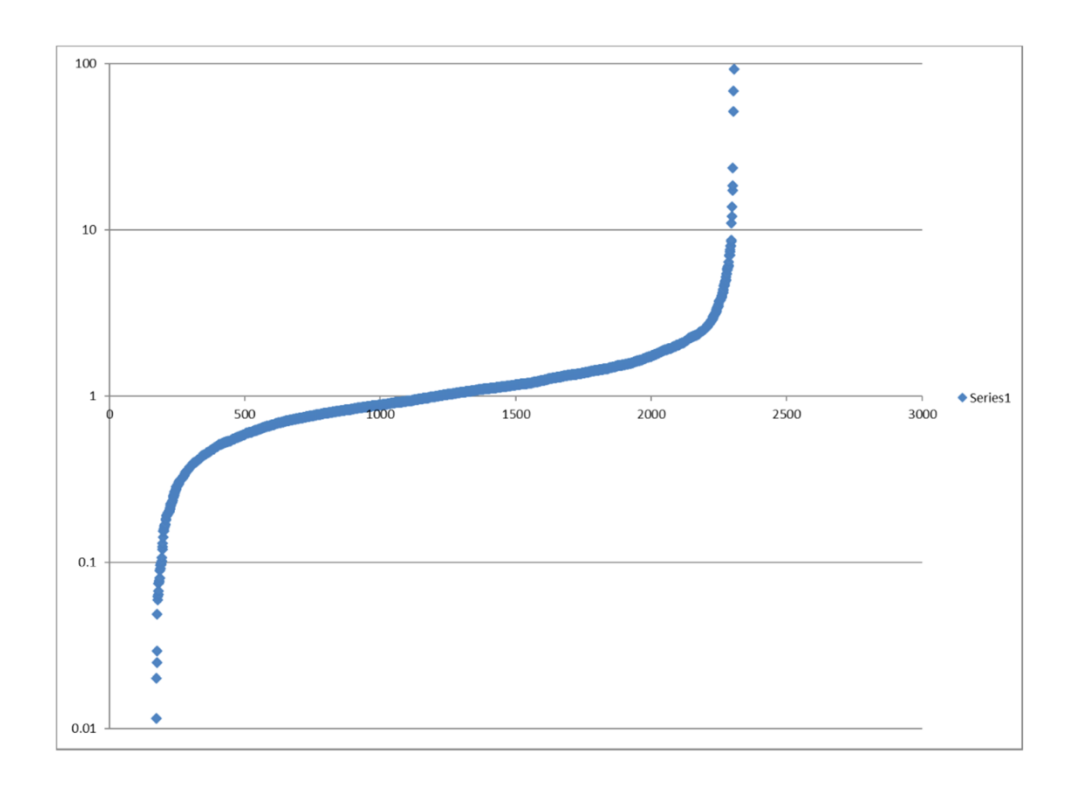


Figure S 7: Quantitative proteomics and Western blot analysis on Oxford co-cultures, related to Figure 2. (A): Representative protein regulation levels in independent experiment SD22, where individual peptides are identified by database search and quantified using spectral counting.



SD22

Figure S 8: Network visualization of Oxford co-cultures from the quantified proteins using Cytoscape (with text mining"/"no evidence" removed), related to Figure 2. Raw protein association data was obtained from STRING. Green nodes represent proteins which are at least 2 fold down-regulated (<0.5), red nodes are proteins which are at least 2 fold up-regulated (>2) and grey nodes are proteins which show less than two-fold variation (between 0.5 to 2). Results for the network condensation analysis using Expressence in SD22 experiment independently. The modules in the figure represent the groups of highest correlated change for the larger network. The node colour is mapped to Measurement values (log transformed MaxQuant intensity values). SD: Sprague Dawley rats.

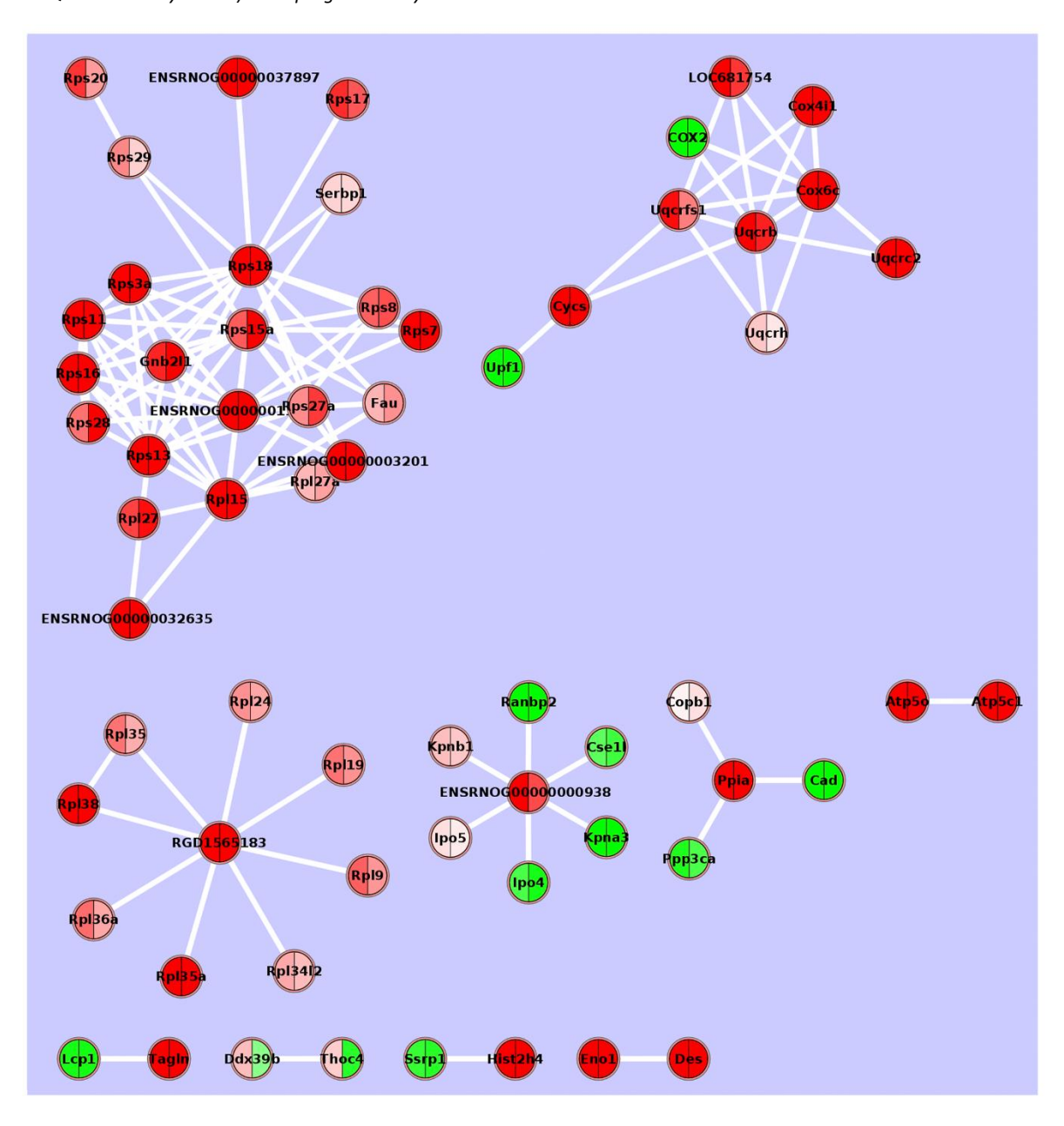


Figure S 9: Quantitative proteomics and Western blot analysis on Oxford co-cultures, related to Figure 2. (A): Representative protein regulation levels in independent experiment SD5, where individual peptides are identified by database search and quantified using spectral counting.

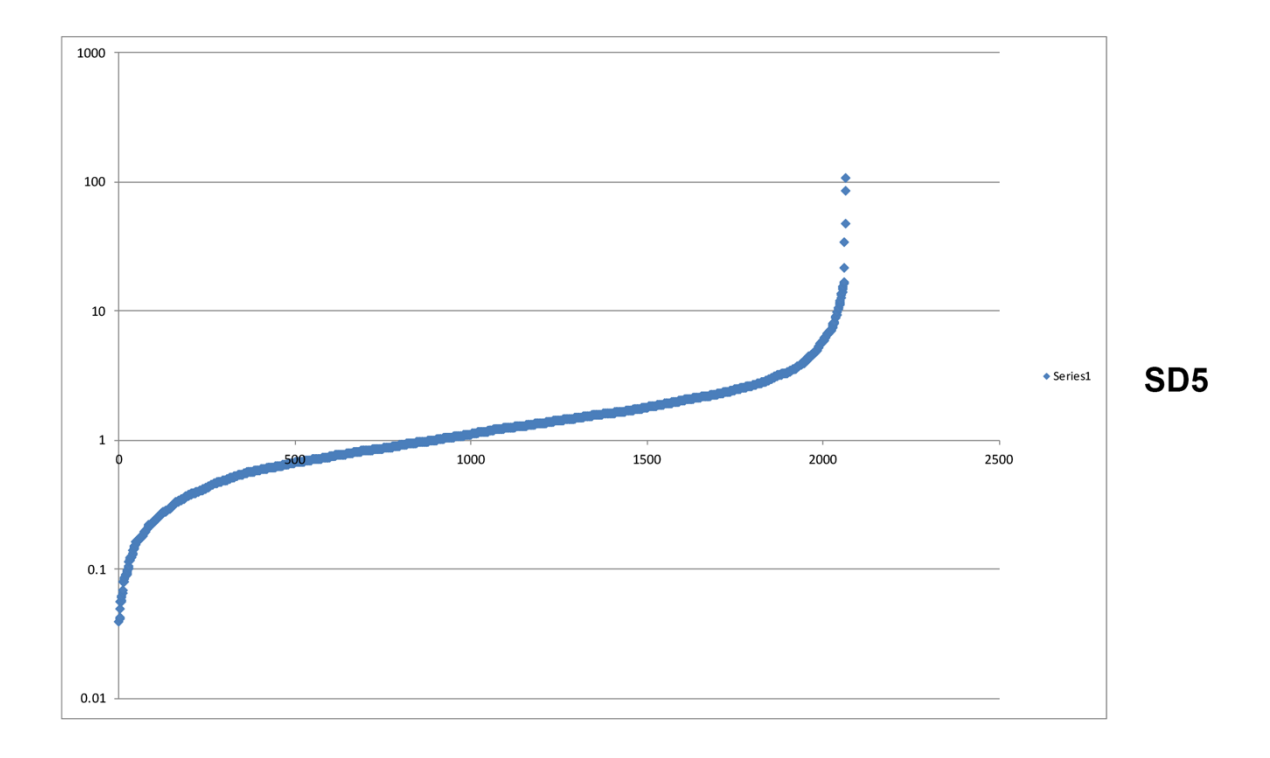


Figure S 10: Network visualization of Oxford co-cultures from the quantified proteins using Cytoscape (with text mining"/"no evidence" removed), related to Figure 2. Raw protein association data was obtained from STRING. Green nodes represent proteins which are at least 2 fold down-regulated (<0.5), red nodes are proteins which are at least 2 fold up-regulated (>2) and grey nodes are proteins which show less than two-fold variation (between 0.5 to 2). Results for the network condensation analysis using Expressence in SD5 experiment independently. The modules in the figure represent the groups of highest correlated change for the larger network. The node colour is mapped to Measurement values (log transformed SINQ intensity values). SD: Sprague Dawley rats.

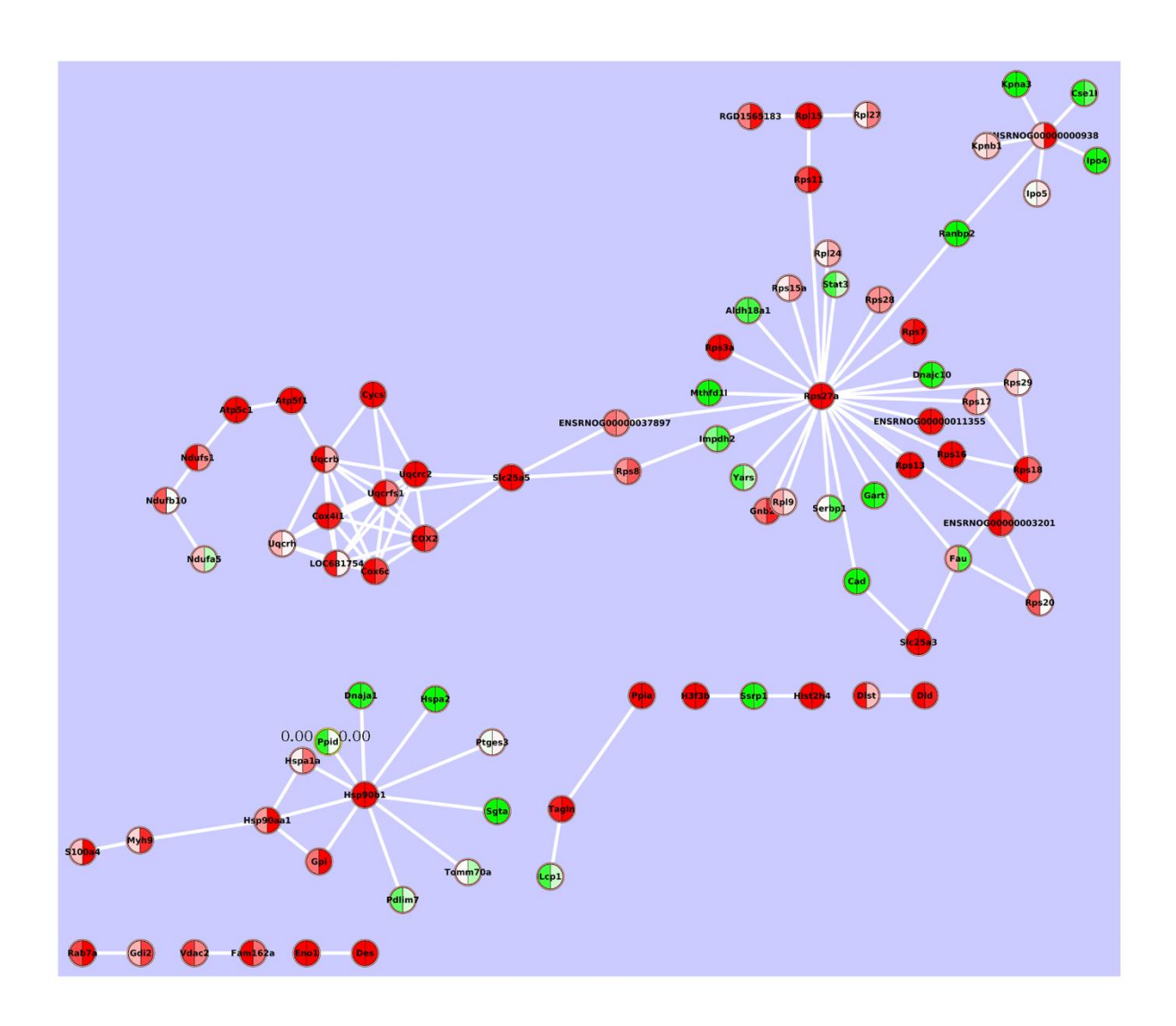


Figure S 11: Western blot analysis and confirmation of protein regulation in two randomly selected proteins from independent Oxford culture experiments (SD22, SD5 and WKY8), related to Figure 2. SD: Sprague Dawley rats, WKY: Wistar Kyoto Rats.

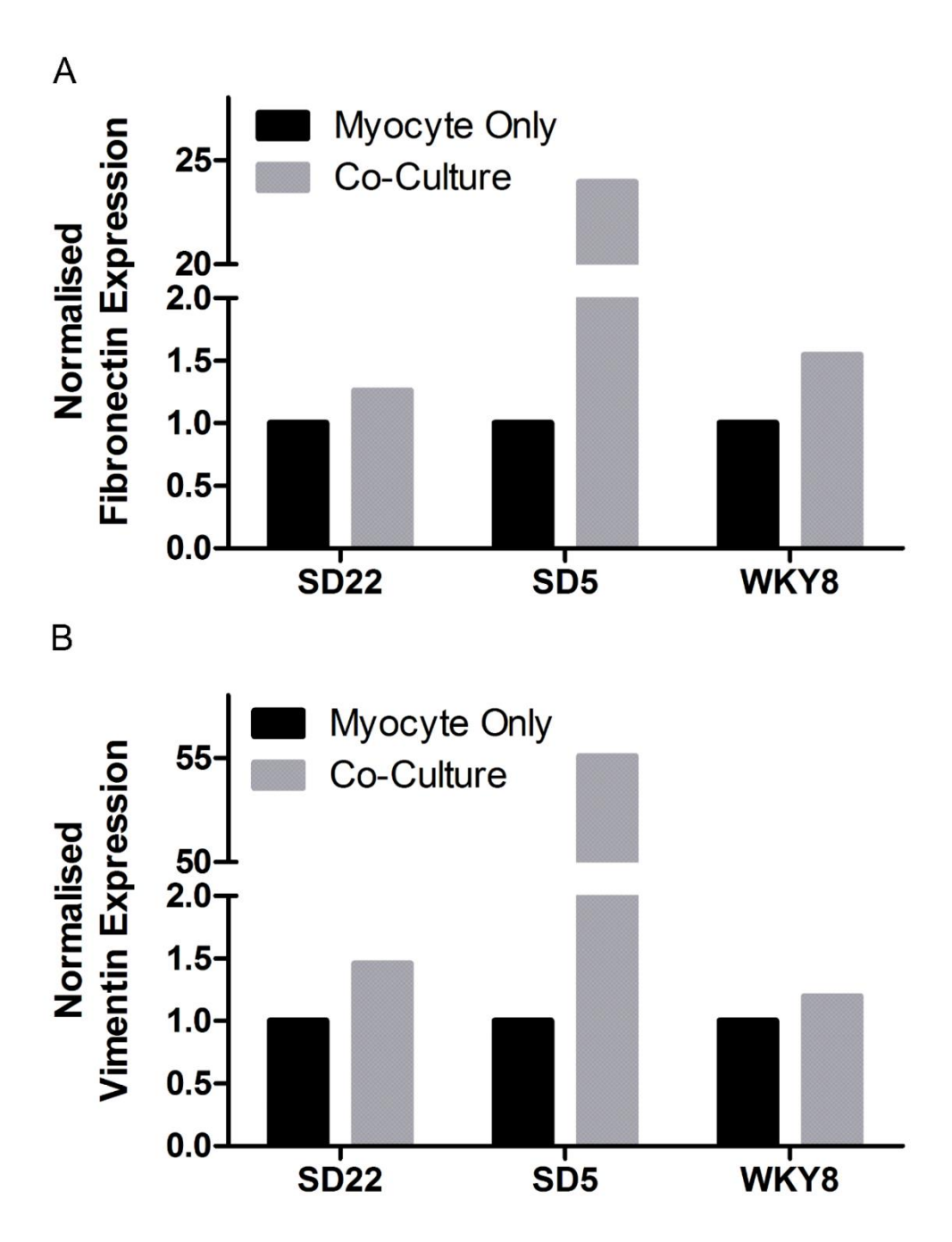


Figure S 12: Western blots of Connexin43 expression in Oxford cultures grown in the absence and presence of sympathetic cardiac stellate neurons in two separate co-culture experiments (SD and WKY), related to Figure 2. SD: Sprague Dawley rats; WKY: Wistar Kyoto Rats.

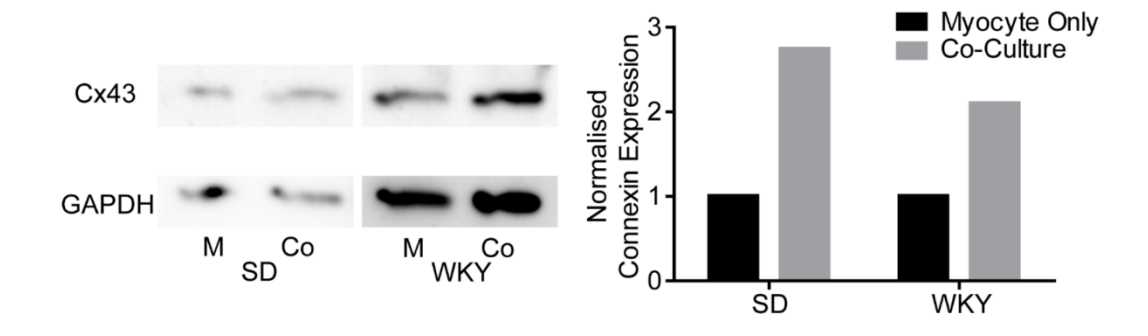


Figure S 13: Effects of sympathetic cardiac stellate neurons on conduction velocity in SBU cardiac/co-cultures using optical mapping (Rhod-4 AM dye) and 1 Hz electrical stimulation, related to Figure 2. Overall, co-culturing myocytes with sympathetic neurons at 3 different concentrations of myocyte-neuron co-cultures did not alter conduction velocity of cardiomyocytes, where average conduction velocities (\pm std dev) were 17.505 \pm 2.92 in myocyte only cultures, 17.092 \pm 4.01 in 20:1 co-cultures, 16.46 \pm 2.91 in 100:1 co-cultures and 20.791 \pm 5.79 in 600k:1 co-cultures; (myocyte only cultures n=6, 20:1 co-cultures n=5, 100:1 co-cultures n=4, 600k:1 co-cultures n=6). Plot of conduction velocity of different SBU co-cultures and myocyte only cultures.

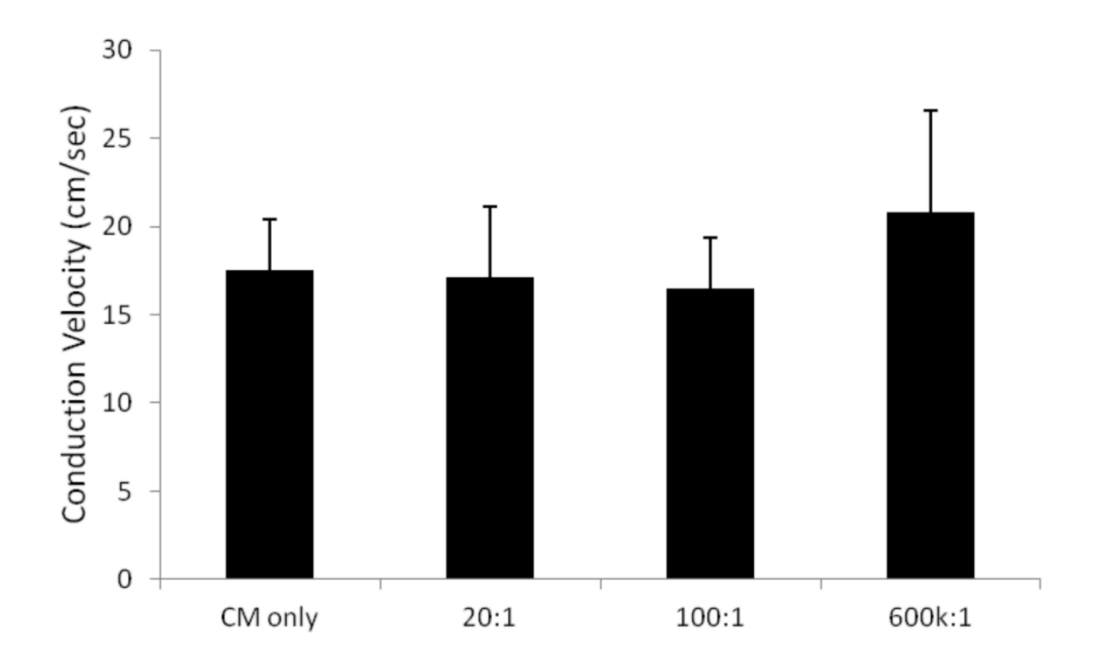
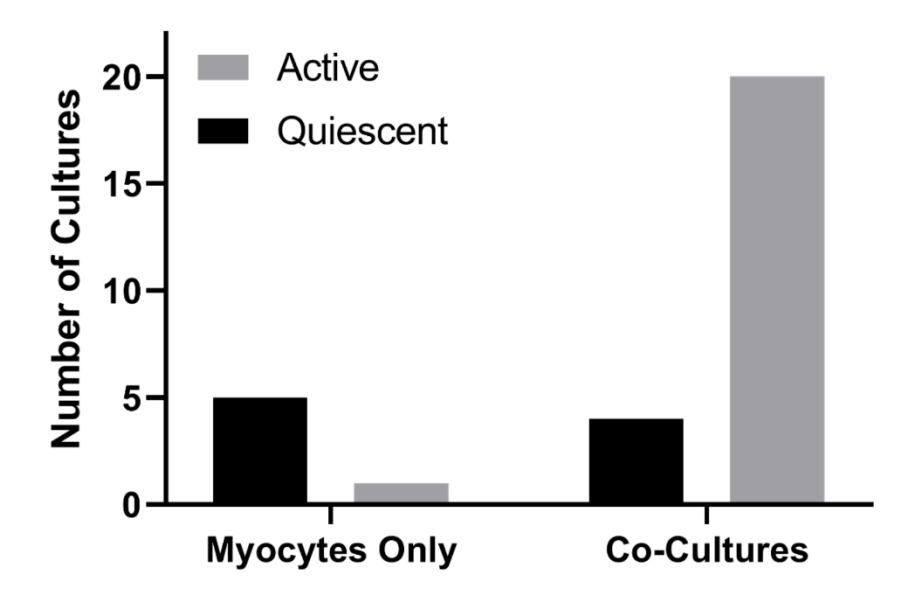


Figure S 14: High throughput fluorescent imaging of co-culture experiments to study the effects of sympathetic cardiac stellate neurons on cardiac activity in well-connected SBU cardiac cultures, related to Figure 5, using optical mapping (cultures loaded with dye Di-4-ANBDQBS). Fishers exact test (two sided), p = 0.0046 statistically significant. n = 6 myocytes and n = 24 for co-cultures.



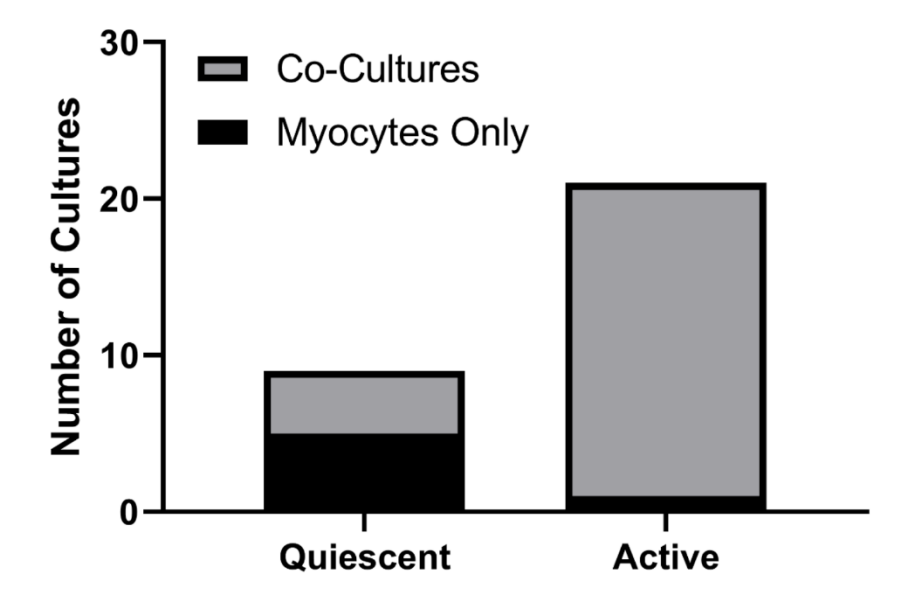


Figure S 15: High throughput fluorescent imaging of SBU co-culture experiments to drive ChR2 stellate sympathetic neurons, related to Figure 5. Co-cultures of neurons and myocytes (loaded with dye Di-4-ANBDQBS spectrally compatible with ChR2). (A and B) Fixed bright field image and YFPChR2 (expressed in the neurons) confocal image of a co-culture (1:5 neuron-myocyte ratio). (C-D) Neuronal stimulation via ChR2, top panel (C) myocyte only culture therefore no beat rate response observed to ChR2 stimulation, bottom panel (D), beat rate response observed during the periods of light stimulation in a co-culture. (E) Post processed traces using custom-written Matlab script. Where, blue is the trace after baseline subtraction and after median filtering, red indicates detected spike times, black is an indicator of when light is present (black down=light off). (F) Neural stimulation via ChR2. (i) Raw traces showing beat rate responses observed in co-cultures, and (ii) no beat rate responses observed in co-cultures that were blocked by the beta blocker metoprolol (10 μM). (iii) Zoomed in region from an action potential response.

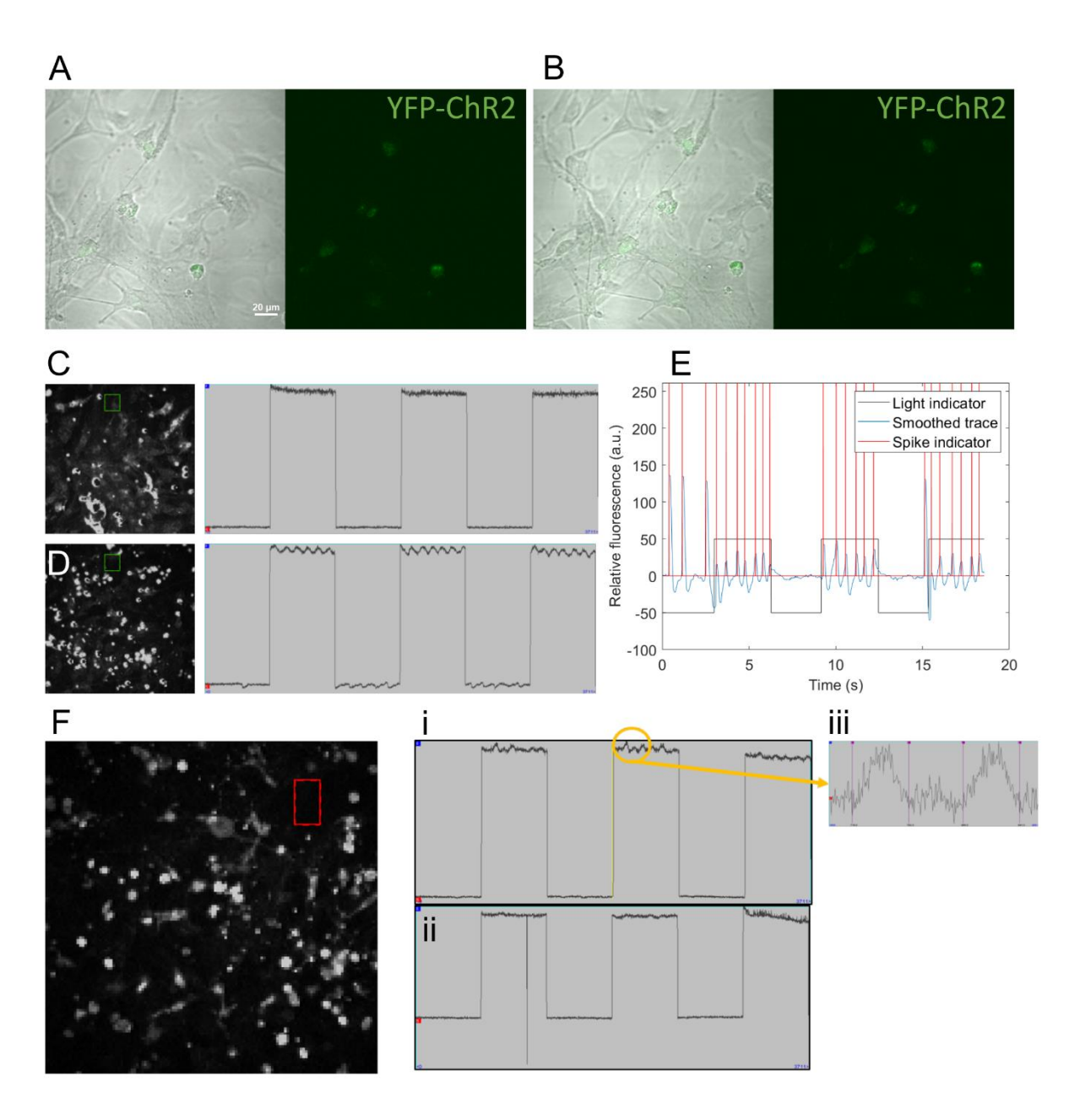


Figure S 16: High throughput fluorescent imaging of SBU cardiac-neuron cultures upon uncaging of nicotine (RuBi-Nicotine from Tocris; related to Figure 5. Panel (A) cardiac only monolayer (control, no neurons). Trace (Ai) full experimental trace, long spike corresponding to flash of light to uncage nicotine. (Aii) Control beat rate prior to uncaging (before light flash); (Aiii) Post-nicotine beat rate after uncaging; (Aiv) Post-nicotine beat rate after 3 minutes. Panel (B) neuron-myocyte co-culture. (Bi) full experimental trace, long spike corresponding to flash of light to uncage nicotine of nicotine; (Bii) Control beat rate prior to uncaging (before light flash); (Biii) Post-nicotine beat rate after uncaging of nicotine; (Biv) Post-nicotine beat rate after 3 minutes. (C-G) Example traces from the different uncaging experiments in the different neuron-myocyte concentration plates. (C) No responses to nicotine were detected in the control myocyte only dishes (representative example). (D) 1:5 neuron-myocyte co-culture. (E) 1:20 neuron-myocyte co-culture. (F) 1:100 neuron-myocyte co-culture. (G) 1:100,000 neuron-myocyte co-culture. Black line indicates moment of blue light flash to uncage the caged nicotine.

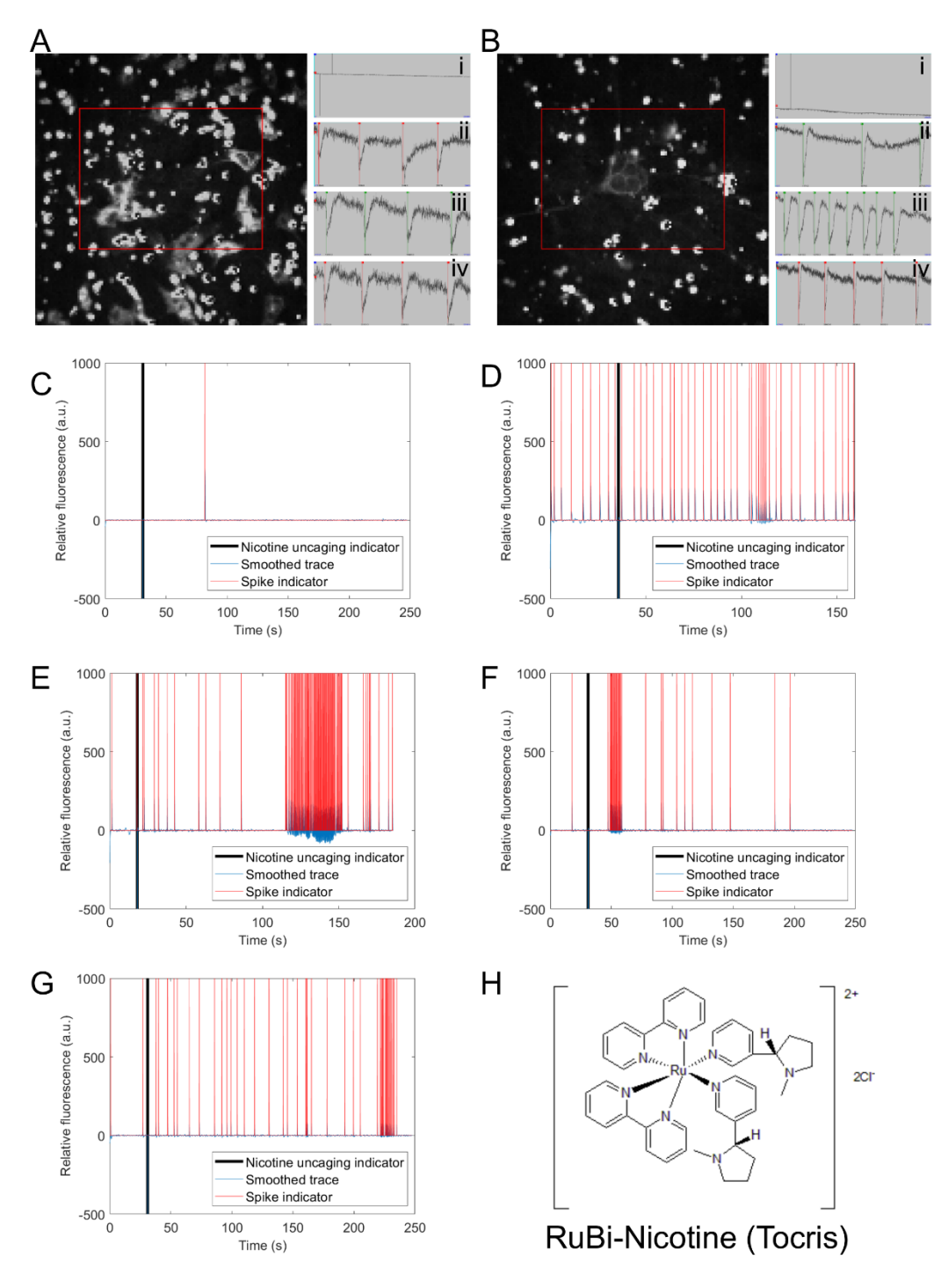


Figure S 17: High throughput fluorescent imaging of SBU co-culture experiments to study the effect of standard nicotine on co-cultures, related to Figure 5. Co-cultures of neurons and myocytes at different neuron to myocyte ratios (A myocyte only, C 1:5, E 1:20, G 1:100 and I 1:100,000) were exposed to 10 μ M nicotine (nicotine response traces B, D, F, H and J,) and the voltage traces were recorded (cultures loaded with dye Di-4-ANBDQBS). Example traces and responses are shown in this figure.

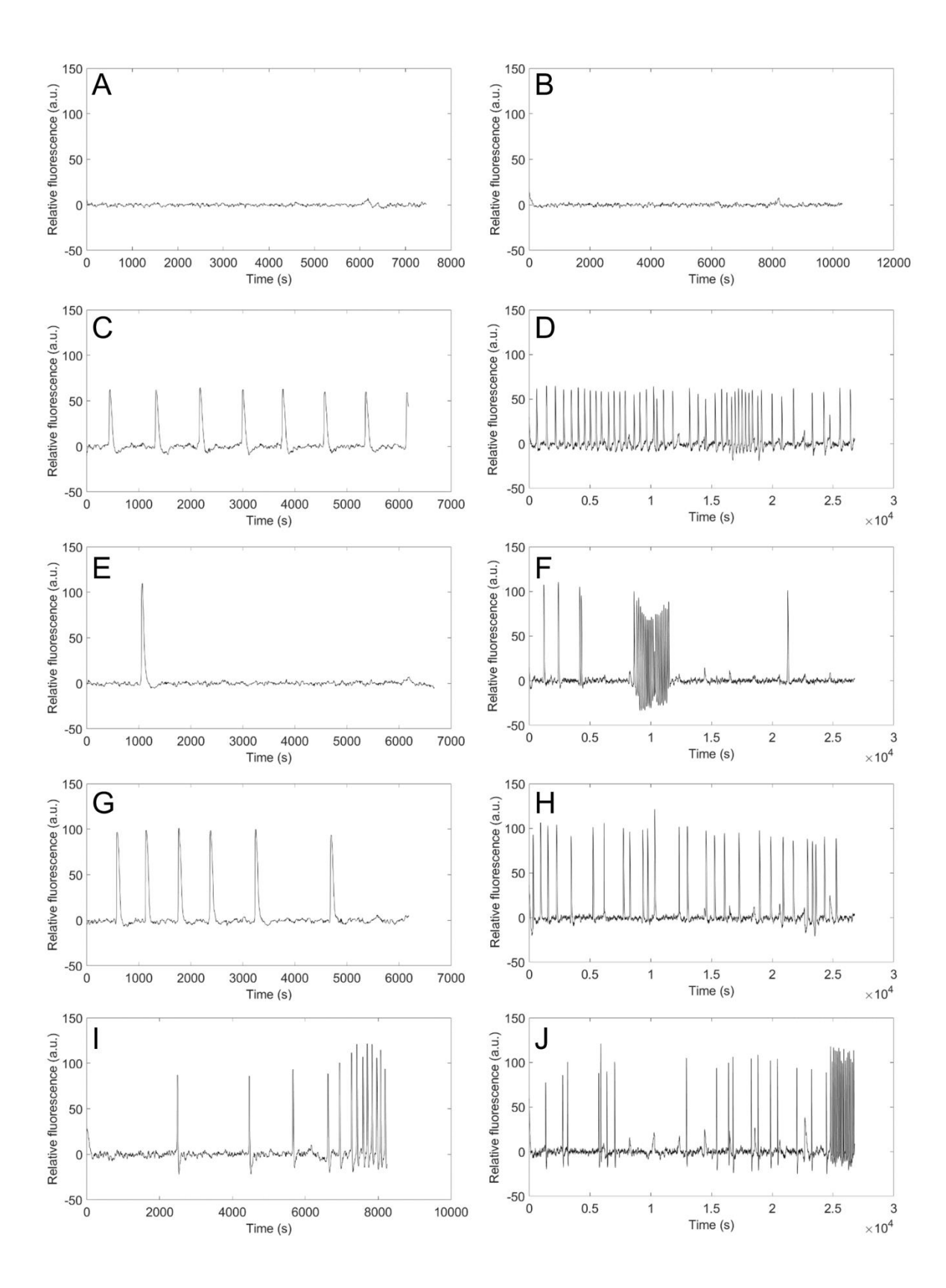


Figure S 18: Pilot co-cultures of Cor.4U cardiomyocytes and Peri.4U hiPSC-derived peripheral neurons (largely sympathetic) developed by Axiogenesis (now Ncardia), related to Figure 5. (A and B) Cardiomyocytes labelled with alpha-actinin staining (green) and DAPI nuclear stain (blue). (C) Peri.4U hiPSC-derived peripheral neurons infected with hChR2-eYFP. (D) Optogenetic neural stimulation of cardiac tissue via Channelrhodopsin2 (ChR2), selectively expressed only in the neurons. Co-cultures of neurons and myocytes (loaded with dye Di-4-ANBDQBS spectrally compatible with ChR2). Optical stimulation (470 nm) was provided at pulse lengths of 3 s, at 0.5 Hz, using irradiance of 0.5-1mW/mm2. Post processed traces using custom-written Matlab software. Traces showing baseline little/no activity and followed by long light pulse stimulation, action potentials are evoked indirectly in the myocytes via the ChR2-light-sensitized neurons. Blue is the trace after baseline subtraction after median filtering, red indicates detected spike times, black is an indicator of when light is present (black up=light off; black down=light on).

